

## Research paper

# Diagenesis and origin of calcite cement in the Flemish Pass Basin sandstone reservoir (Upper Jurassic): Implications for porosity development



Di Xiong <sup>a,\*</sup>, Karem Azmy <sup>a</sup>, Nigel J.F. Blamey <sup>b</sup>

<sup>a</sup> Department of Earth Sciences, Memorial University of Newfoundland, St. John's, NL, A1B 3X5, Canada

<sup>b</sup> Department of Earth Sciences, Brock University, St. Catharines, ON, L2S 3A1, Canada

## ARTICLE INFO

### Article history:

Received 12 May 2015

Received in revised form

6 August 2015

Accepted 18 November 2015

Available online 23 November 2015

### Keywords:

Sandstone

Calcite cement

Diagenesis

Geochemistry

Clastic reservoir

Flemish Pass Basin

## ABSTRACT

The Flemish Pass Basin is a deep-water basin located offshore on the continental passive margin of the Grand Banks, eastern Newfoundland, which is currently a hydrocarbon exploration target. The current study investigates the petrographic characteristics and origin of carbonate cements in the Ti-3 Member, a primary clastic reservoir interval of the Bodhrán Formation (Upper Jurassic) in the Flemish Pass Basin.

The Ti-3 sandstones with average Q<sub>86.0</sub>F<sub>3.1</sub>R<sub>10.9</sub> contain various diagenetic minerals, including calcite, pyrite, quartz overgrowth, dolomite and siderite. Based on the volume of calcite cement, the investigated sandstones can be classified into (1) calcite-cemented intervals (>20% calcite), and (2) poorly calcite-cemented intervals (porous). Petrographic analysis shows that the dominant cement is intergranular poikilotopic (300–500 µm) calcite, which started to form extensively at early diagenesis. The precipitation of calcite occurred after feldspar leaching and was followed by corrosion of quartz grains. Intergranular calcite cement hosts all-liquid inclusions mainly in the crystal core, but rare primary two-phase (liquid and vapor) fluid inclusions in the rims ((with mean homogenization temperature ( $T_h$ ) of  $70.2 \pm 4.9^\circ\text{C}$  and salinity estimates of  $8.8 \pm 1.2$  eq. wt.% NaCl). The mean  $\delta^{18}\text{O}$  and  $\delta^{13}\text{C}$  isotopic compositions of the intergranular calcite are  $-8.3 \pm 1.2\text{\textperthousand}$ , VPDB and  $-3.0 \pm 1.3\text{\textperthousand}$ , VPDB, respectively; whereas, fracture-filling calcite has more depleted  $\delta^{18}\text{O}$  but similar  $\delta^{13}\text{C}$  values. The shale normalized rare earth element (REE<sub>SN</sub>) patterns of calcite are generally parallel and exhibit slightly negative Ce anomalies and positive Eu anomalies. Fluid-inclusion gas ratios (CO<sub>2</sub>/CH<sub>4</sub> and N<sub>2</sub>/Ar) of calcite cement further confirms that diagenetic fluids originated from modified seawater. Combined evidence from petrographic, micro-thermometric and geochemical analyses suggest that (1) the intergranular calcite cement precipitated from diagenetic fluids of mixed marine and meteoric (riverine) waters in suboxic conditions; (2) the cement was sourced from the oxidation of organic matters and the dissolution of biogenic marine carbonates within sandstone beds or adjacent silty mudstones; and (3) the late phases of the intergranular and fracture-filling calcite cements were deposited from hot circulated basinal fluids.

Calcite cementation acts as a main controlling factor on the reservoir quality in the Flemish Pass reservoir sandstones. Over 75% of initial porosity was lost due to the early calcite cementation. The development of secondary porosity (mostly enlarged, moldic pores) and throats by later calcite dissolution due to maturation of organic matters (e.g., hydrocarbon and coals), was the key process in improving the reservoir quality.

© 2015 Elsevier Ltd. All rights reserved.

## 1. Introduction

Calcite cement is a significant factor controlling sandstone

reservoir quality through reduction of porosity and permeability. However, when it starts to form during early stages of diagenesis, it provides a framework that may resist burial compaction and retains porosity until decarbonatization at greater depth (Hesse and Abid, 1998; Liu et al., 2014). Earlier studies have documented early-formed calcite cement and examined its origin by traditional geochemical method, such as stable isotope and major and minor

\* Corresponding author.

E-mail address: [dx6150@mun.ca](mailto:dx6150@mun.ca) (D. Xiong).

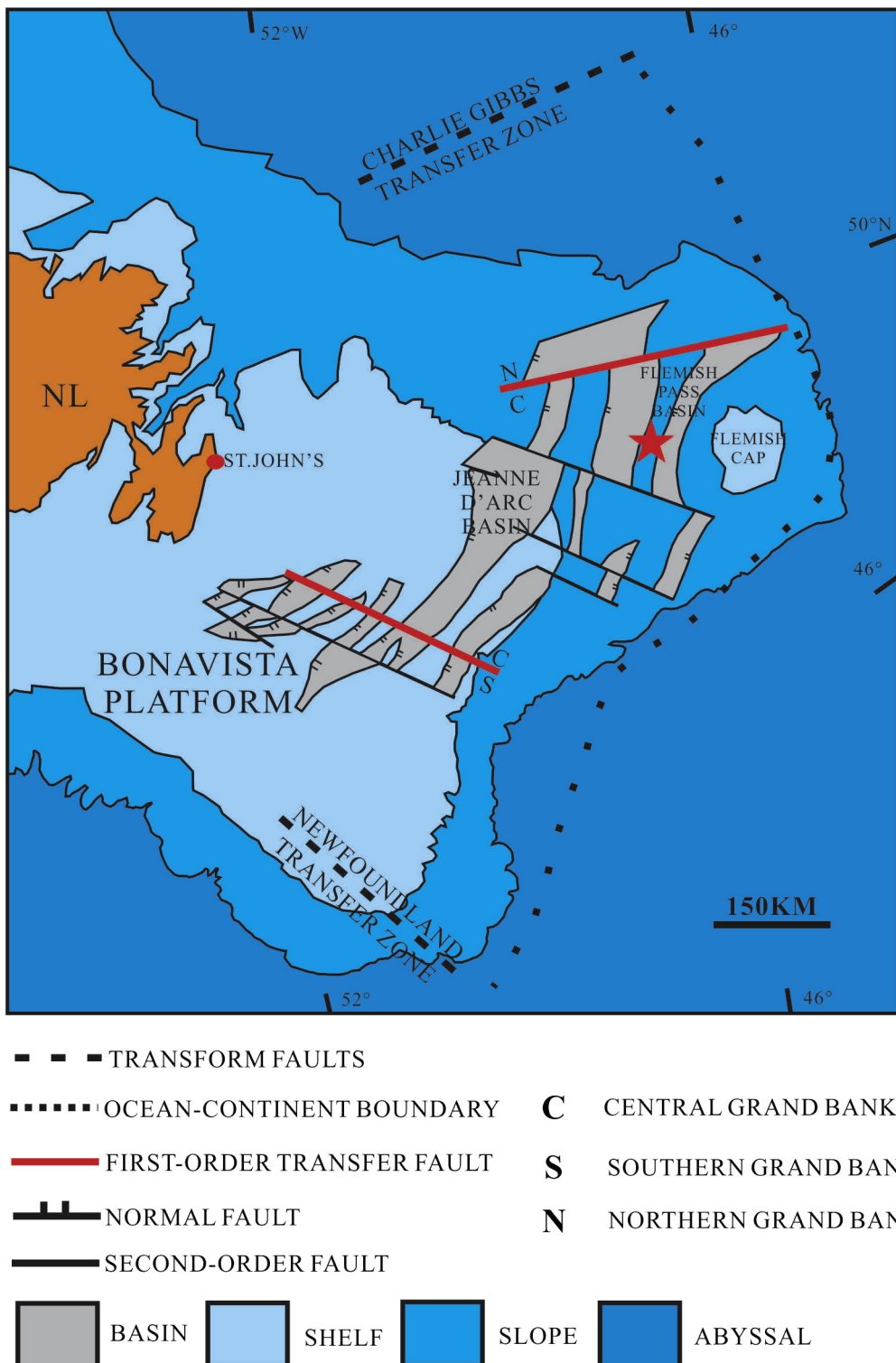


**Fig. 1.** Mesozoic sedimentary basins and structures of offshore Newfoundland and location of the Flemish Pass Basin (modified from Tankard and Welsink, 1989; Hesse and Abid, 1998; Normore, 2006; Lowe et al., 2011).

element analysis (e.g., Saigal and Bjørlykke, 1987; Brown et al., 1989; Hesse and Abid, 1998; Baker et al., 2000; McBride et al., 2003; Odigi and Amajor, 2010; García-García et al., 2013; Nyman et al., 2014). However, very recent studies (Azmy et al., 2011) investigated that the utilization of the rare earth element (REE) in

carbonates to better understand their diagenetic environment and REEs have been found to be a useful proxy in studying the origin of diagenetic fluids in sedimentary rocks (e.g., Azmy et al., 2011; Azomani et al., 2013).

Unlike fluid-inclusion microthermometric data, fluid-inclusion

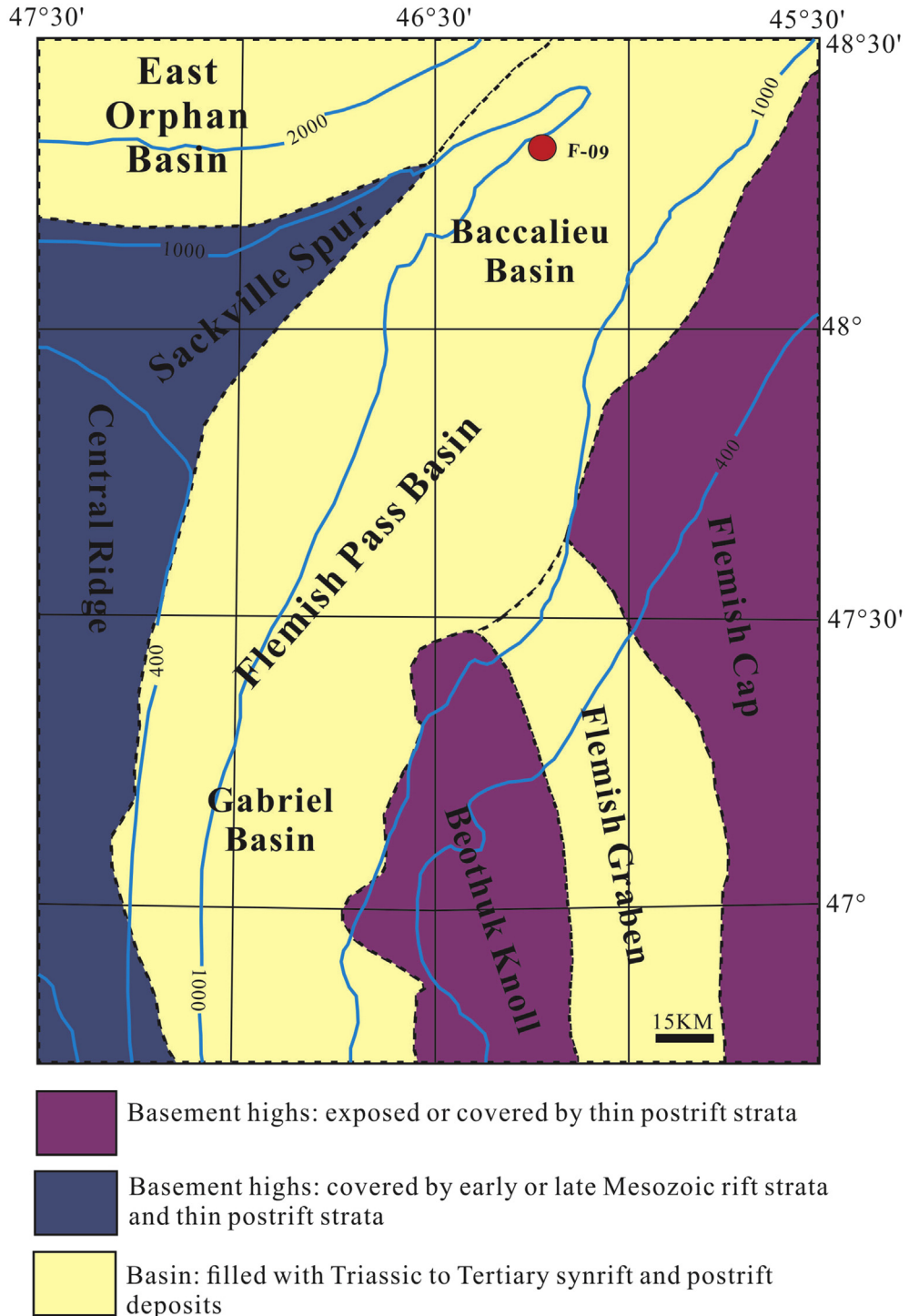


**Fig. 2.** Tectono-structural subunits of the Flemish Pass Basin and approximate location of the Statoil Mizzen F-09 well ( $48^{\circ}18'22.51''$  and  $W46^{\circ}15'57''$ ) (modified from Enachescu, 1987).

gas composition was just recently applied to resolve the origin of diagenetic fluids in sedimentary environment (e.g., Azmy and Blamey, 2013). Studies show that major, minor and noble gases trapped in inclusions during diagenesis document the chemical characteristics of the parent fluid, which can provide additional information to discriminate the source of diagenetic fluids (e. g., meteoric, basinal or magmatic) (e.g., Giggenbach, 1986; Norman and Musgrave, 1994; Norman and Moore, 1999; Blamey and

Norman, 2002; Norman et al., 2002). This quantitative gas analysis have recently been tested on non-altered and altered carbonates from different basins and diagenetic settings (Azmy and Blamey, 2013). The relative concentrations of gases can be utilized to reconstruct origin of diagenetic fluids.

The Flemish Pass sandstones of the Bodhrán Formation (informal name) a potential target for hydrocarbon exploration in eastern offshore Newfoundland (Hogg and Enachescu, 2007;

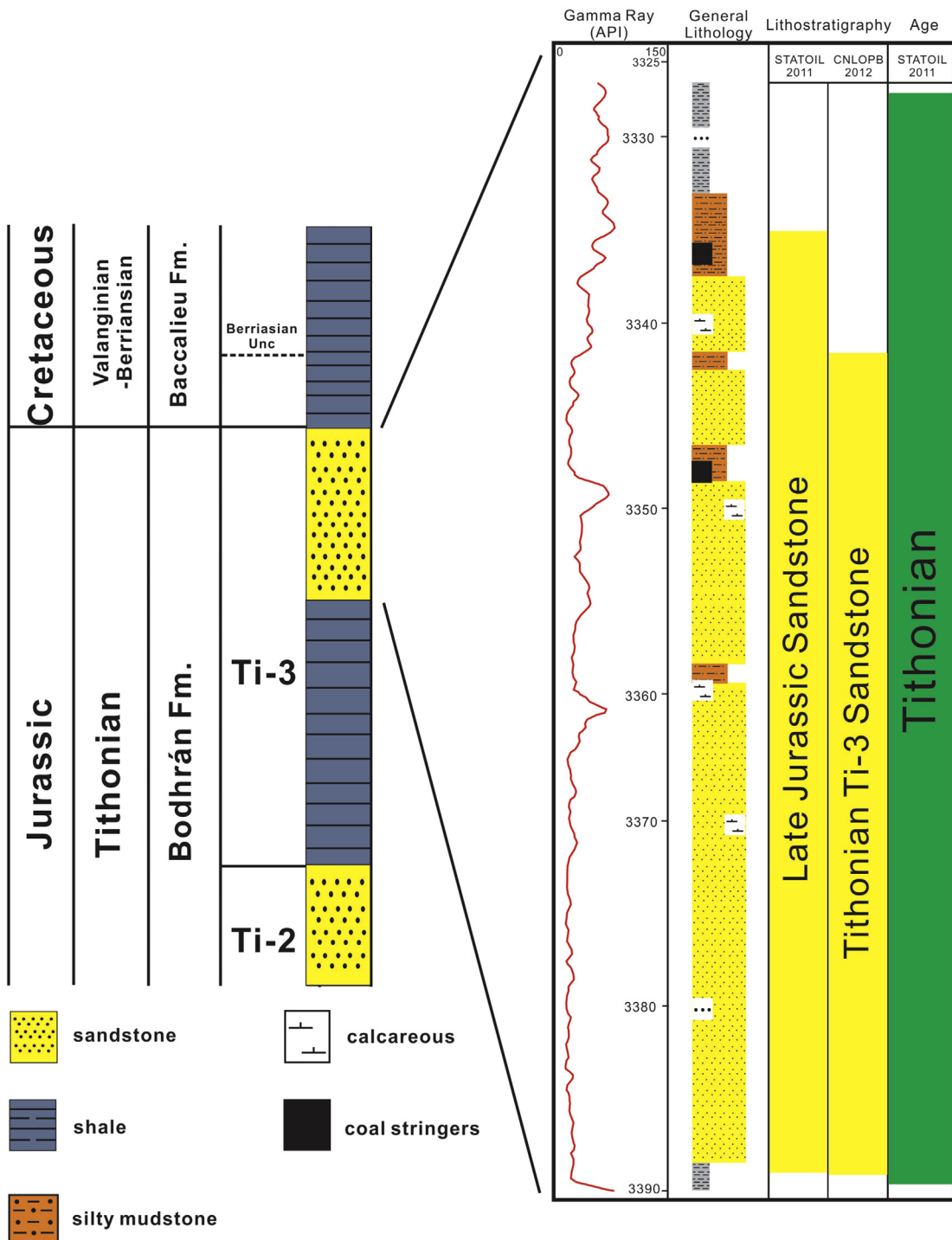


**Fig. 3.** Simplified stratigraphic framework of the Mizzen F-09 well and combined gamma-ray, lithologic, lithostratigraphic and biostratigraphic logs for the Ti-3 Member (the Bodhrán Formation). Data acquired from Natural Resources Canada website ([http://basin.gdr.nrcan.gc.ca/index\\_e.php](http://basin.gdr.nrcan.gc.ca/index_e.php)) and Statoil Canada Resources (2011).

Enachescu et al., 2010; Enachescu, 2014) and calcite has been reported to be the most prevalent cement (Haynes et al., 2013). Although few papers have been published on aspects of the geological history of the Flemish Pass Basin (Foster and Robinson, 1993; DeSilva, 1999; Enachescu et al., 2005; Lowe et al., 2011; McDonough et al., 2011), no major petrographic and diagenetic studies have yet investigated the reservoir sandstones. Thus, unraveling the origin and diagenetic environment of calcite cement is a significant issue for better understanding and predicting

porosity distribution, which may therefore assist in future hydrocarbon exploration and production.

The current investigation focuses on the origin of calcite cementation in the Upper Jurassic Ti-3 sandstones (informal name) of the Bodhrán Formation of the Flemish Pass Basin by using a multitechnique approach of petrographic, microthermometric, fluid-inclusion gas ratios, and geochemical analyses. The main objectives of the study are:

- (1) to identify the diagenetic evolution and reservoir characterization of the sandstones in Flemish Pass Basin,
- (2) to investigate and reconstruct the paragenetic sequence of multiple diagenetic events, and
- (3) to elucidate the origin of the carbonate cements and their influence on porosity development and distribution.

## 2. Geological setting

The east coast of Newfoundland formed as a passive continental margin during the Mesozoic separation of Pangaea and the sequential spreading of the Atlantic. The intracontinental double-failed rift arm produced a series of variably interconnected syn-rift basins spanning from Late Triassic to Late Cretaceous and corresponding to extensional and thermal subsidence stages (Enachescu, 1987, 1988; Tankard and Welsink, 1989; Foster and Robinson, 1993; Sinclair, 1993). Those half-graben basins are confined to down-to-the-east basin bounding fault (Murre/Mercury fault) associated with antithetic and synthetic faults, and separated by pre-Mesozoic basement highs. The tectonic activity has evolved into major three rift stages accompanied with salt tectonics, and variable rates of deposition and erosion (Enachescu, 1987; Sinclair, 1995). The initial rifting phase (Late Triassic to Early Jurassic) resulted in the break-up of North America and Africa; the second rifting phase (Late Jurassic to Early Cretaceous) recorded the separation of the Grand Banks from Iberia; and the last rifting episode (Early Cretaceous, Barremian-Albian) involved the division of North Europe craton from Canada and propagation in Labrador Sea.

The Flemish Pass Basin is situated approximately 485 km east of St. John's, Newfoundland (Fig. 1), formed during Late Triassic-Early Jurassic (the North Atlantic rifting stage) on the continental passive margin of the Grand Banks. The basin covers about 30,000 km<sup>2</sup> at water depths ranging from 400 to 1100 m (Foster and Robinson, 1993; DeSilva, 2000; Huppertz and Piper, 2009; Lowe et al., 2011). This deep-water basin was divided into two depocenters, the Baccalieu subbasin in the North and the Gabriel subbasin in the South (DeSilva, 1999). The basin is confined to the east by the basement high of the Flemish Cap and Beothuk Knoll, to the north by the Cumberland Ridge, to the south by the Avalon Uplift, and separated from the Jeanne d'Arc Basin to the Southwest by the Central Ridge (Fig. 2; Foster and Robinson, 1993; Enachescu, 1987). Sackville Spur, a major sediment drift, extends from the northeasternmost Grand Banks slope down onto the basin floor of Flemish Pass (Kennard et al., 1990). The investigated Mizzen F-09 well (48°18'22.51"N, 46°15'57"W) was drilled by Statoil Canada Ltd. and Husky Energy in mid-2011 and penetrated into sandstones of the Bodhrán Formation (Fig. 3) of Upper Jurassic (Tithonian), which were found to be a good quality clastic reservoir (Haynes et al., 2013; Enachescu, 2014). The underlain Tithonian shales have been considered as the equivalent of source rocks in the Rankin Formation (Enachescu, 2012). The potential of the

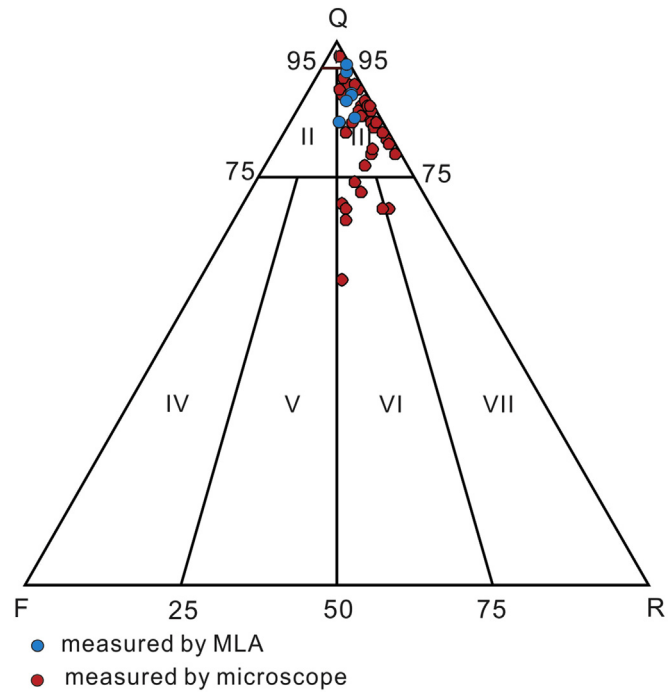


**Fig. 4.** QFR triangular diagram of sandstone petrography showing the composition of the Ti-3 sandstones Folk (1980). Q, quartz; F, feldspar; R, rock fragments. Blue symbols represent results from MLA and red symbols are visual estimates from thin-section using conventional optical microscope. (For interpretation of the references to color in this figure legend, the reader is referred to the web version of this article.)

undiscovered recoverable petroleum resources in the basin has been calculated at 1.7 billion barrels, with expected field sizes ranging 44 to 528 million barrels (Hogg and Enachescu, 2007).

The Bodhrán Formation sandstones is divided into five Members (from base to top Ti-0 to To-4), among which the Ti-3 Member (informal name), which is deemed to be a primary reservoir interval (Haynes et al., 2013). The sediments of Ti-3 Members consist of two stages, fluvial deposits in the lower section, and fine upward to estuarine deposits (Haynes et al., 2013). The Ti-3 sandstones have been classified into six main lithofacies, from bottom to top include: well-sorted matrix-supported gravel to cobble conglomerates; fine-to coarse-grained sandstone with isolated, well-rounded conglomerates and siltstone rip-ups; fine-to medium-grained sandstones with occasional mudstone drapes and common carbonaceous laminae; interbedded shales, siltstones and fine-grained sandstones (Haynes et al., 2013).

## 3. Methods

One hundred and ten core samples were collected from the Ti-3 sandstones of the borehole Mizzen F-09 (sampling interval ~0.5 m).

**Table 1**

Mineralogic composition (in %) of the Ti-3 sandstones determined by the MLA.

Sample#	Quartz (%)	Plagio-Feldspar	K-Feldspar	Lithic Fragment	Calcite	Dolomite	Pyrite	Illite	Mica	Chlorite	Other eavy minerals	Others
3344	48.6	1.0	1.3	5.7	39.2	0.1	0.5	0.7	1.7	0.1	0.4	0.8
3367	52.0	0.5	0.6	3.2	40.6	0.1	0.9	0.2	0.8	0.1	0.4	0.6
3368	74.8	1.0	1.2	6.6	3.0	0.5	8.8	0.8	2.2	0.2	0.4	0.5
3377.1	77.0	0.7	0.4	3.8	5.3	0.3	9.7	0.5	1.2	0.2	0.2	0.7
3382.8	48.5	0.9	0.6	4.4	41.4	0.7	0.8	0.2	1.1	0.2	0.2	1.0
3387.4	81.6	2.3	1.4	6.9	2.6	0.1	0.6	1.1	2.0	0.2	0.4	0.9

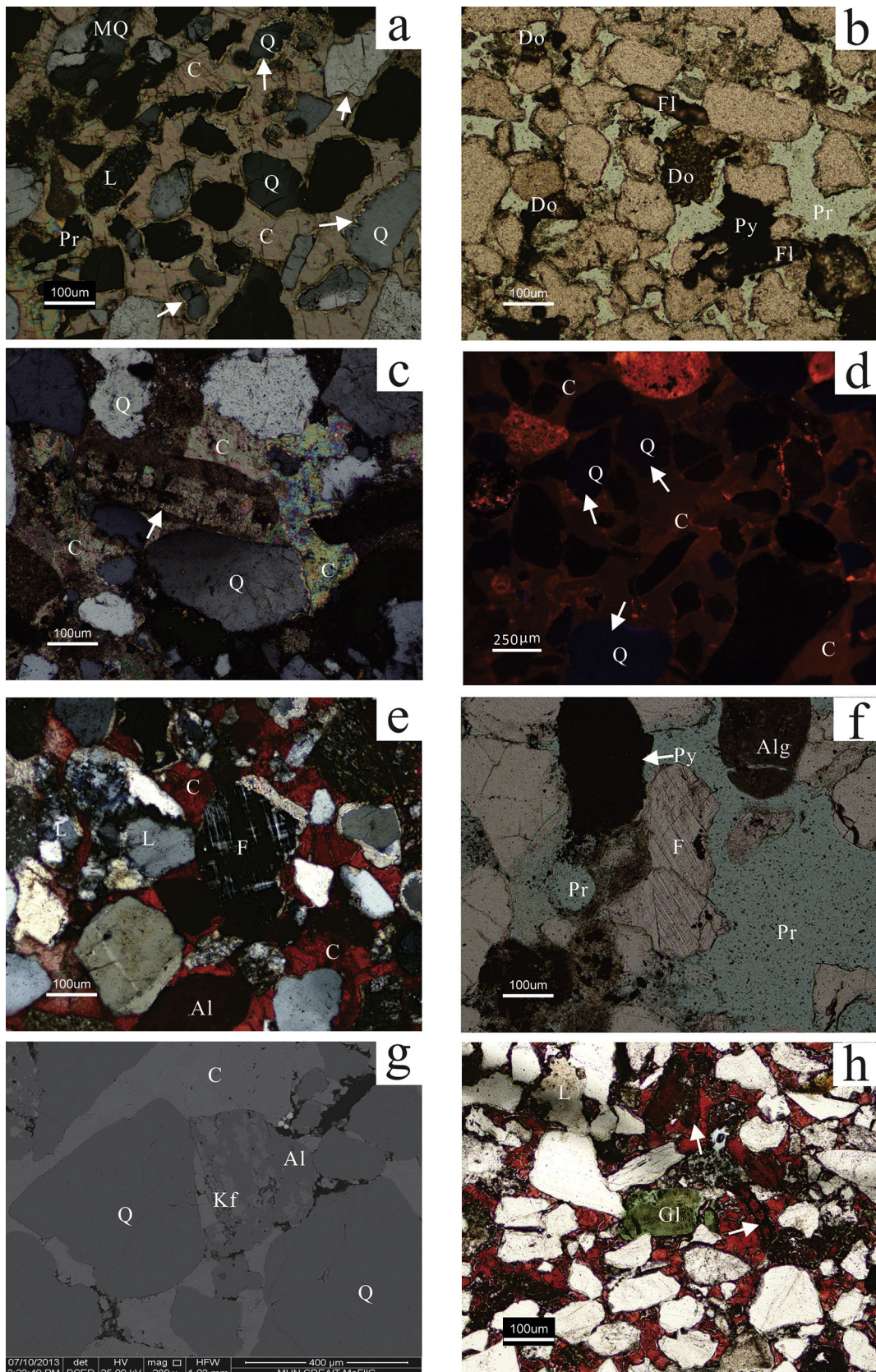


**Fig. 5.** Photomicrographs of petrographic features of the Ti-3 sandstones. (a) Sandstone extensively cemented by early, poikilotopic calcite cement (C). Quartz grains (Q) corroded by calcite cements, showing pitted margin and embayment (arrows). Metamorphic quartz (MQ) and lithic fragment (L) engulfed by calcite cements. Sandstone showing grain "floating" texture and high intergranular volumes (>30%). Secondary pore (Pr) resulting from dissolution of calcite cements (left), Sample# 3371.1, crossed polars, (b) Secondary pore (Pr) formed by calcite dissolution. Authigenic dolomite (Do) aggregates and rhombs scattering in interstitial spaces after calcite dissolution. Subhedral pyrite (Py) replacing fossil fragments (Fl), Quartz grains (Q) also displaying corrosion feature. Sample# 3339.3, polarized light, (c) A few monocrystalline quartz grains (Q) exhibiting sweeping extinction.

**Table 2**

Estimated porosity, calcite cement contents, and stable carbon and oxygen isotopic data of calcite cements. V1, V2, and V3 values refer to measurements of fracture-filling calcites.

Sample#	$\delta^{13}\text{C}_{\text{VPDB}}$	$\delta^{18}\text{O}_{\text{VPDB}}$	Porosity %	Calcite %	Sample#	$\delta^{13}\text{C}_{\text{VPDB}}$	$\delta^{18}\text{O}_{\text{VPDB}}$	Porosity %	Calcite %
3335.6	-0.7	-8.9	1	45	3369.4	-3.2	-8.2	2	33
3339.3			15	0	3369.9	-2.8	-5.3	3	26
3340.6	-3.9	-10.6	6	32	3371.1	-3.1	-9.0	2	46
3341.9			18	0	3372.5	-3.4	-7.9	1	34
3342.6	-4.4	-11.0	2	40	3374	-2.0	-8.5	1	32
3343.6			22	0	3375	-2.8	-9.0	1	34
3344.6	-1.2	-7.1	1	47	3375.85	-4.2	-8.9	10	34
3348.6			8	5	3377.1			20	0
3351.3	-1.3	-7.2	1	36	3377.9	-4.8	-8.1	7	37
3354.2			18	0	3379.7	-4.3	-7.5	3	42
3355.6			15	7	3381.1	-2.6	-9.1	2	40
3356.4			7	0	3382.2			17	3
3357.2	-0.7	-8.4	1	40	3382.8			2	41
3357.7			20	0	3383.4			7	39
3360.4	-4.1	-7.8	4	32	3384.5			12	19
3361.1			14	0	3384.8	-2.5	-8.7	3	39
3362.6			17	0	3385.7	-3.0	-7.2	2	40
3361.6			15	0	3386.5	-4.7	-8.0	1	41
3363.4	-3.9	-7.9	4	37	3387.4			20	0
3364.2			28	0	3387.8			23	0
3365.9	-0.1	-7.7	1	36	V1	-2.1	-10.8		
3367.8	-3.5	-8.2	1	46	V2	-1.8	-10.7		
3368.6			18	0	V3	-2.2	-10.7		

All samples were thin sectioned for petrographic examinations. Mirror-image slabs from each thin section were polished and cleaned before microsampling and geochemical analyses. The thin sections were impregnated with blue epoxy to facilitate the identification of pore spaces (e.g., Blamey et al., 2014). They were also stained with Alizazin Red-S and postassium ferricyanide solutions to recognize the carbonate cement types (Lindholm and Finkelman, 1972).

Thin sections were examined under a Nikon Eclipse E600POL microscope with  $4 \times$ ,  $10 \times$ , and  $20 \times$  lenses to identify mineral composition as well as petrographic and diagenetic features, and to quantify cement and porosity contents. Photomicrographs were taken by an attached Nikon DXM 1200F digital camera. Cathodoluminescence was performed on polished thin sections to identify the cement generations by using a Technosyn cold cathodoluminoscope at  $\sim 12\text{kV}$  accelerating voltage and  $\sim 0.7\text{ mA}$  current intensity. Ultraviolet luminescence (UL) was performed using a CRAICQDI 202 UV unit mounted on a Zeiss imager D1m microscope.

Six representative thin sections were selected for quantitative mineral liberation analysis (MLA), which was conducted using the FEI MLA 650F scanning electron microscope (SEM) facility at Memorial University of Newfoundland (MUN). The technique relies on backscattered electron imaging to distinguish grain boundaries, and uses various x-ray emissions to classify grains of different minerals. This analysis can identify minerals within polished rock thin-sections and yield various results on mineral characteristics, such as abundance, size and texture.

Microthermometric analysis was conducted on ten double-polished wafers from calcite-cemented samples (intergranular

and fracture-filling) using a Likham THMSG 600 heating-freezing conjunction with an Olympus BX51 microscope. Calibration was done on a monthly basis using a  $\text{CO}_2$  standard for  $-56.6\text{ }^\circ\text{C}$  whereas a water standard was used for ice melting at  $0.0\text{ }^\circ\text{C}$  and the critical point at  $374.1\text{ }^\circ\text{C}$ . Microthermometric measurements of homogenization temperature ( $T_h$ ), initial melting temperature ( $T_i$ ) and final melting temperature of ice ( $T_m(\text{ice})$ ) of fluid inclusions were performed following procedures outlined by Shepherd et al. (1985). Aqueous fluid salinities were estimated using  $T_m(\text{ice})$  and the equation modified by Bodnar (2003).

Additionally, fluid-inclusion gas analysis was run on samples using the incremental crush fast scan method (e.g., Azmy and Blamey, 2013; Blamey et al., 2014) following the procedures described in detail by Blamey (2012). Samples were cleaned with alkaline solutions to remove surface organics, rinsed several times with deionized water and dried at room temperature. Samples were crushed incrementally under a vacuum of  $\sim 10\text{--}8\text{ Torr}$  producing 6 to 10 successive bursts. Data acquisition was carried out by means of two Pfeiffer Prisma quadrupole mass spectrometers (Blamey et al., 2014). Routinely, the system analyses for the following:  $\text{H}_2$ ,  $\text{He}$ ,  $\text{CH}_4$ ,  $\text{H}_2\text{O}$ ,  $\text{N}_2$ ,  $\text{O}_2$ ,  $\text{H}_2\text{S}$ ,  $\text{Ar}$ ,  $\text{CO}_2$ ,  $\text{C}_2\text{H}_4$ ,  $\text{C}_2\text{H}_6$ ,  $\text{SO}_2$ ,  $\text{C}_3\text{H}_6$ ,  $\text{C}_3\text{H}_8$ ,  $\text{C}_4\text{H}_8$ ,  $\text{C}_4\text{H}_{10}$ , and benzene (Blamey et al., 2014). The analysis was calibrated with commercial gas mixtures, in-housed fluid inclusion gas standards as described by Norman and Blamey (2001). The concentration of each species is calculated by proprietary software to provide a quantitative analysis. Precision for the major gas species  $\text{CO}_2$ ,  $\text{CH}_4$ ,  $\text{N}_2$ , and  $\text{Ar}$  is better than 5% (cf. Azmy and Blamey, 2013).

Analysis of C- and O-isotopes were performed on selected

Minor fibrous and sparry calcite (arrow) growing inside a bioclast, Sample#3365.9, crossed polars, (d) Cathodoluminescope image showing dull to bright CL of poikilotopic calcite cements (C) and bluish CL (arrows) of some quartz grains (Q). Grains mainly showing point contacts and at times grain contacts, Sample# 3367.8, (e) Feldspar (F, microcline) with chessboard twinning showing partial dissolution and replacement by calcite cement. Calcite cement (C) and algal micrite (Al) stained dark red. Metamorphic lithic fragments (L), Sample# 3386.5, crossed polars, (f) Remnant of extensively replaced feldspar (F, perthite) in the center. Dissolved calcite leaving enlarged and moldic pores (Pr). Spherulitic and subhedral pyrite (Py) replacing bioclasts, such as algae (Alg), Sample# 3387.8, polarized light, (g) SEM image revealing albited K-feldspar (Kf) engulfed by calcite cement (C), patchy albite (Al) in dark shades of grey and K-feldspar (Kf) in light shades of grey, Sample# 3382.2, SEM, (h) Minor deformed glauconite (Gl) occurring in the sandstones. Fossil fragments (arrows) replaced by diagenetic calcite. Sedimentary lithic fragment (L, mudstone) to the left also showing corrosion features, Samples# 3357, polarized light. (For interpretation of the references to color in this figure legend, the reader is referred to the web version of this article.)

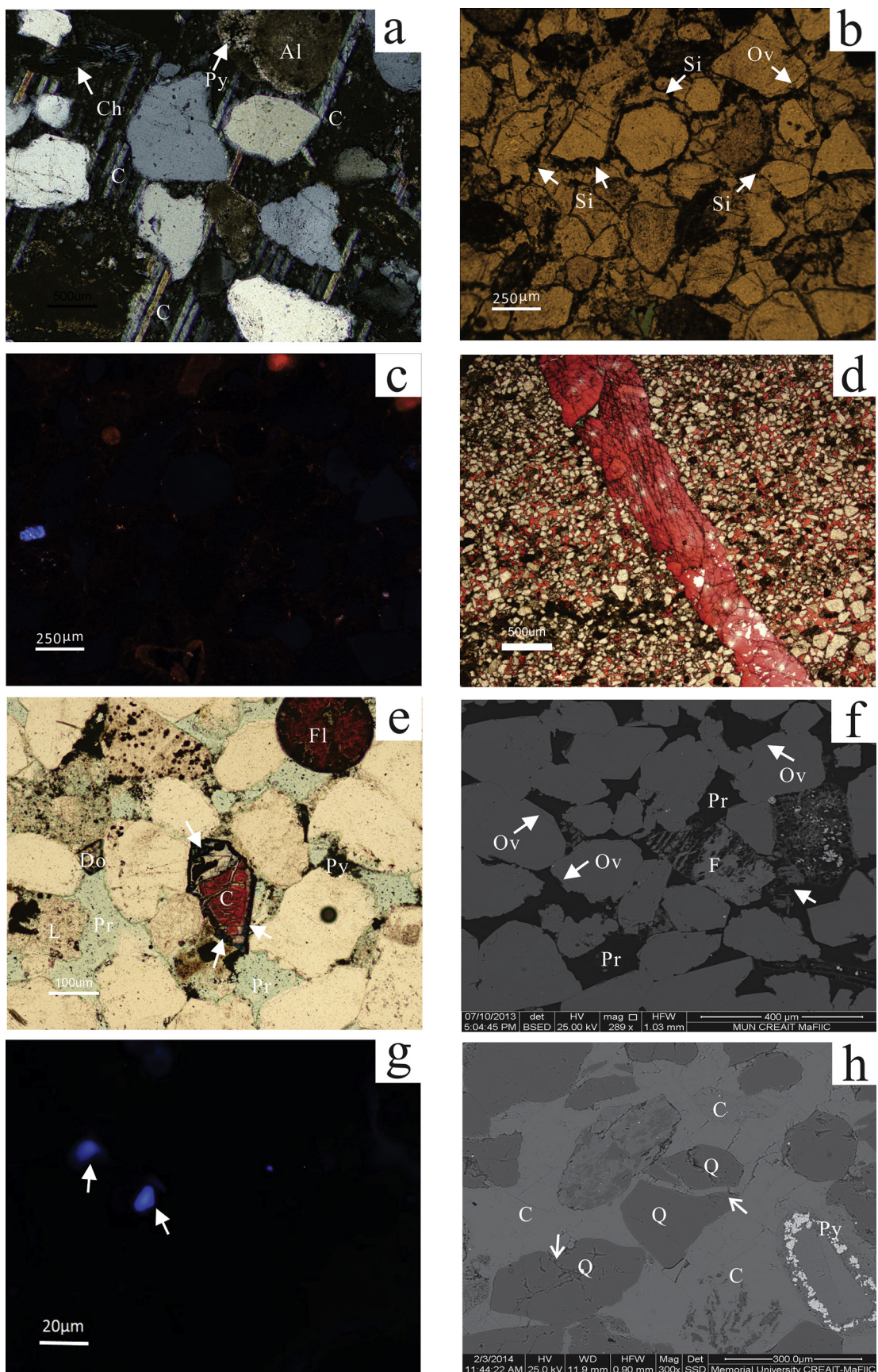


**Fig. 6.** Photomicrographs of petrographic features of the Ti-3 sandstones. (a) Twinning planes of calcite cements occurring uninterruptedly on either side of grains. Poikilotopic calcite cement engulfing chlorite (Ch) and algal micrite (Al), Sample# 3365.9, crossed polars. (b) Authigenic siderites (Si) scattered on the poikilotopic calcite cement. Grain-rimming

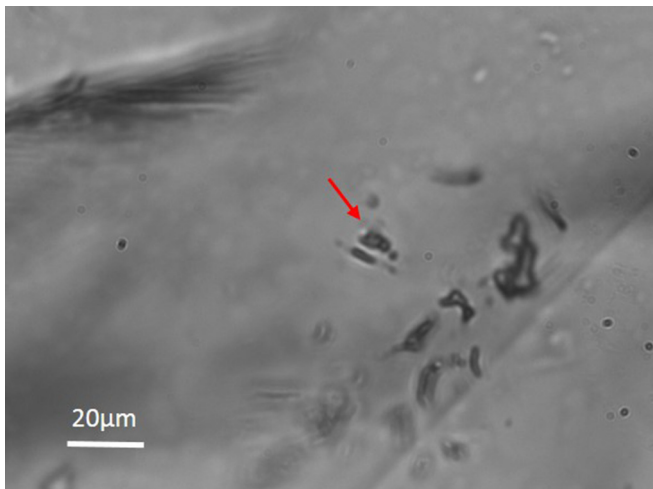


**Fig. 7.** Photomicrographs of primary fluid inclusions in calcite cement from Ti-3 sandstones. Irregular-shaped mono-phase fluid inclusions likely occur in clusters (left), while rare two-phase fluid inclusions generally occur individually in the crystal rim (arrow).

samples with high volume of calcite cement by  $\text{CO}_2$  liberation method. Polished slabs were cleaned with deionized water and dried before microdrilling. About 0.8 mg–2.5 mg microsamples were drilled from each corresponding mirror-image slabs by a low-speed microdrill. The powder samples were collected in the glass vials, and reacted in inert atmosphere with ultrapure orthophosphoric acid at 50 °C in the Thermo-Finnigan Gas bench II. The  $\text{CO}_2$  extracted from samples was carried by helium through chromatographic column and transferred to Thermo Finnigan DELTA V Plus isotope ratio mass spectrometer, in which the gas was ionized and measured for isotopic ratios. Analytical errors of better than 0.1‰ ( $2\sigma$ ) for the analyses were determined by repeated measurements of CBM ( $\delta^{18}\text{O} = -8.58\%$  and  $\delta^{13}\text{C} = +0.75\%$  vs. VPDB), NBS-19 ( $\delta^{18}\text{O} = -2.20\%$  and  $\delta^{13}\text{C} = +1.95\%$  vs. VPDB), and MUN-CO-1 ( $\delta^{18}\text{O} = -13.40\%$  and  $\delta^{13}\text{C} = -21.02\%$  vs. VPDB) during each run.

Major, minor and rare earth elements (REE) were analyzed by the Secondary Ion Mass Spectrometry (SIMS) at MUN. The  $^{16}\text{O}^-$  ions was accelerated at a few kV and shot onto a gold-coated polished sample mount. Samples were “sputtered” to generate “secondary” ions that were detected by the mass spectrometer (Denniston et al., 1997). All samples were measured based on international and in-house standards (<http://www.mun.ca/research/resources/creait/physical-sci/maf/sims.php>). Samples were bombarded with an ion beam of  $\text{O}^-$  (5–15  $\mu\text{m}$  wide) at 15–20 nA and 10 kV. Each spot was pre-sputtered for 120 s with a 25  $\mu\text{m}$  square raster applied to the beam, then sputtered again using a 10  $\mu\text{m}$  raster for 100 s. Positively charged sputtered secondary ions were transmitted into the mass spectrometer through a potential of 4.5 keV. To minimize interference, the instrument was operated at an energy offset of 80 eV with a Medium Contrast Aperture (150  $\mu\text{m}$ ) and Entrance and Exit Slits paired to give flat topped peaks at a Mass Resolving Power

(MRP) of 2975. Count time was dependent of measured elements varied between 2 and 6 s. OKA-C (calcite from Oka carbonatite complex, Quebec) and NBS 610 standards were analyzed by SIMS and compiled results were compared to those by Gladney et al. (1987). The precision expressed as the relative standard deviation of the SIMS equipment is reasonably good: <6% for Mn, Sr, La, Ce, Nd, Dy and Sm while it is <20% for Fe, Yb and Y. The REE concentrations were then normalized based on Post-Archen Australian Shale (McLennan, 1989).

## 4. Results

### 4.1. Sandstone petrography

Based on Folk's (1980) sandstone classification scheme (Table 1, Appendix I) the Ti-3 sandstones plot generally within the field of sublitharenites ( $Q_{86.0} F_{3.1} R_{10.9}$ ) of high mineralogical maturity. However, few data points may plot within the fields of quartzarenites and a few feldspathic litharenite (Fig. 4). The detrital grains are moderately sorted, fine-to medium-grained, angular to sub-rounded, presenting tangential, flattened and rarely concavo-convex grain contacts. Authigenic minerals include, in order of abundance, calcite, pyrite, quartz overgrowth, dolomite and siderite. The Ti-3 sandstones can be generally classified, based on the contents of calcite, into intervals with extensive calcite cement and poor porosity (Fig. 5a and Appendix I) and others with poor calcite and high volume of irregularly distributed pores (Fig. 5b and Appendix I). The porosity is largely secondary (enlarged and moldic pores), depending on the degree of dissolution, and ranges from 1% to 28% (Table 2). Enlarged pores are common in the high-porosity sandstone intervals and mainly originate from the dissolution of cements, while moldic pores occur commonly in the calcite-cemented sandstone intervals of bioclasts.

Detrital quartz is predominantly monocrystalline with straight extinction, but some monocrystalline quartz grains exhibit sweeping extinction (Fig. 5c). A few quartz grains were sourced from plutonic or high-grade metamorphic rocks, since they appear blue to reddish-brown CL (Fig. 5d) under the cathodoluminescope (e.g., Boggs and Krinsley, 2006; Seyedolali et al., 1997). Moreover, a few (less than 2% of total quartz grains) polycrystalline quartz grains with sutured boundaries occur. Quartz grains normally exhibit corroded texture and embayment boundaries (Fig. 5a, b) and quartz overgrowths are not common particularly in the calcite-cemented sandstone intervals.

The feldspar content is generally low (<4%; Table 1, Appendix I) and K-feldspars and plagioclases are approximately equal in amount. Nearly all feldspars show alteration features, partially dissolved or replaced by calcite (Fig. 5e, f). Fibrous or lathy illite can be traced around altered feldspars. In addition, MLA analysis reveals some albitionization on K-feldspars (Fig. 5g), where albites replace K-feldspars as patches, and grow parallel to cleavage planes in parent grains.

Lithic fragments are mainly of sedimentary origin, including cherts, mudstones and silty clasts (Fig. 5h). Metamorphic rock fragments (MRF) occur frequently in the lower part of the Ti-3

spherulitic siderite (Si) and siderites (Si) growing into the corroded margin of detrital quartz (arrows). Minor quartz exhibiting early overgrowth (Ov) enclosed by calcite cement, Sample# 3385.7, polarized light, (c) Cathodoluminescence image of (b) showing dull CL of sediment components form cemented intervals containing siderite, Sample# 3385.7, (d) Fracture-filling calcites, Sample# 3357.2, polarized light, (e) Minor dolomite (arrows) on calcite cement remnants. Late pyrite cements (Py) filling intergranular spaces. Fossil fragment (Fl), possibly crinoid (stained), Sample# 3387.7, polarized light, (f) Quartz overgrowths (Ov) frequently occurring in the uncemented intervals. Altered K-feldspar (F) showing partial dissolution texture on albited lamellae. Lathy illite (right arrow) produced from altered feldspar. Concavo-convex grain contacts and remnants of dissolved bioclasts to the right, Sample# 3387.4, SEM, (g) Bluish ultraviolet fluorescence seldom showing in calcite cement, Sample# 3367.8, (h) Microcracks occurring in some quartz grains (arrow). Quartz fracture healed by calcite cement (arrow). Note the high intergranular volumes (>35%) in cemented intervals and early fine pyrite (Py) starting to replace a bioclast, Sample# 3344.6, SEM.

**Table 3**

Statistics of microthermometric measurements of calcite cements in the Ti-3 sandstones.

Type		$T_h$ °C	$T_m$ (ice) °C	Eq. wt% NaCl
Poikilotopic calcite (All-liquid inclusion)	n	27	27	
	Mean	-1.7	3.0	
	S.D	1.1	1.7	
	Max	-0.3	6.5	
	Min	-4	0.5	
Poikilotopic calcite (liquid- vapor inclusion)	n	27	13	13
	Mean	72.3	-5.8	8.8
	S.D	5.4	1	1.2
	Max	83.1	-4	11.2
	Min	63.9	-7.6	7.2
Fracture-filling calcite	n	16	8	8
	Mean	101.0	-6.7	10.0
	S.D	21.5	1.6	1.8
	Max	138.1	-5.8	11.5
	Min	75.3	-9.3	8.9

**Table 4**

The weighted mean values of fluid-inclusion gas from sandstone samples with high volume of calcite cements by the incremental crush method. The ratios of N<sub>2</sub>/Ar and CO<sub>2</sub>/CH<sub>4</sub> of quartz are proposed by Blamey et al. (2014).

Sample#	N <sub>2</sub>	Ar	CO <sub>2</sub>	CH <sub>4</sub>	N <sub>2</sub> /Ar	CO <sub>2</sub> /CH <sub>4</sub>
3334.8	0.7436	0.0079	1.564	2.7185	94.17	0.57
3344.5	0.7391	0.0101	3.8043	1.7506	73.11	2.17
3367.8	1.1577	0.0217	5.0362	4.8585	53.25	1.04
3377.9	0.7015	0.0109	3.5181	2.8247	64.21	1.24
3379.7	1.0251	0.0198	7.8036	6.4294	51.70	1.21
3381.1	0.1295	0.0021	0.6956	0.2817	61.70	2.47
Quartz*	0.3403	0.0073	5.2802	0.0564	48.07	96.84

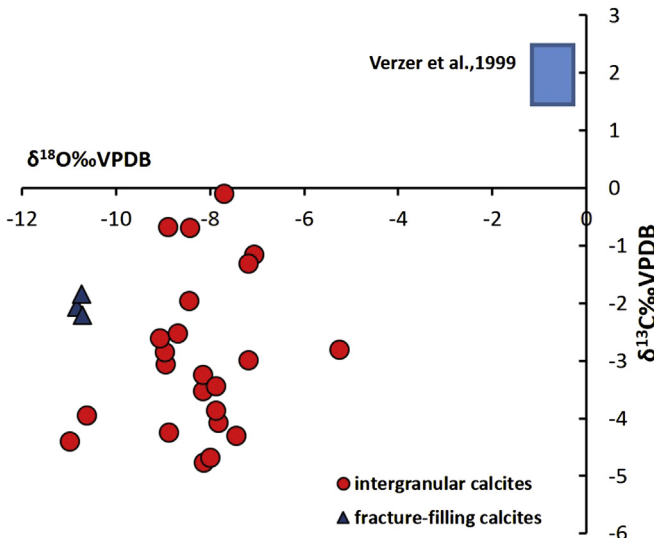


**Fig. 8.** Scatter diagram of  $\delta^{18}\text{O}$  vs.  $\delta^{13}\text{C}$  for calcite cements. The square represents the estimated range of isotopic composition of well-preserved marine carbonates during the Tithonian Stage (Veizer et al., 1999).

sandstones (Fig. 5e). Accessory Minerals include minor glaucnate, chlorite and carbonate grains (Figs. 5h and 6a). Heavy minerals such as pyrite, rutile, apatite, titanite, epidote, staurolite and zircon, are scattered in the Ti-3 sandstones. Bioclasts, of algae, brachiopod, echinoderm and crinoid, are also present and they exhibit signs of replacement and dissolution.

#### 4.2. Carbonate cements

Three types of carbonate cements were generally identified in the Ti-3 sandstones, a high volume of calcite but rare dolomite and siderite.

##### 4.2.1. Calcite

Calcite is the dominant pore-occluding cement in the sandstones. The calcite constitutes up to 47% of the rock volume (Table 2). It occurs mainly as poikilotopic (300–800  $\mu\text{m}$ ; Fig. 5a, d), but rarely as early fibrous on bioclasts (Fig. 5c). The poikilotopic calcite appears in the lowermost intervals, engulfing the majority of grains, and partially replaces feldspars and quartz. The MLA study indicates that calcite is ferroan, which is consistent with the uniformly distributed dark red stain in the thin sections (Fig. 5e). The twinning planes of this calcite appear uninterruptedly on either side of framework grains and bioclasts (Fig. 6a). All poikilotopic calcite cements exhibits uniform CL (dull/moderate to bright) without concentric zoning (Fig. 5d). However, the calcite crystals exhibit dull to no CL particularly when sandstone intervals contain siderites (Fig. 6b,c).

Fracture-filling calcite cements (375–1400  $\mu\text{m}$ ; Fig. 6d) are rare throughout the Ti-3 sandstones. They fill in one fracture with 0.8–14 mm width, which locates within well-cemented sandstones of lower stratigraphic levels of the borehole. The intensity of stain color is identical to that of poikilotopic calcite (dark red) thus suggesting the fracture-filling calcite is also iron-rich (e.g., Lindholm and Finkelman, 1972).

##### 4.2.2. Dolomite

Rare dolomite cements (<2%) fill in the interstitial spaces between quartz grains in the sandstones that have no pervasive calcite cement. It occurs as fine-crystalline dolomite aggregates (80–100  $\mu\text{m}$ ) and individual euhedral to subhedral ferroan dolomite rhombs (35–180  $\mu\text{m}$ ) but might develop as overgrowth around calcite remnants (Figs. 5b and 6e).

##### 4.2.3. Siderite

Siderite cement is rare (<1%) and occur in the lower section of the Ti-3 sandstones, at about 3385 m deep, as very fine grained, dark spherulite crystal rim around some detrital grains (Fig. 6b).

#### 4.3. Quartz cement

Silica cement occurs as syntaxial euhedral overgrowths (average 2.3%) on some detrital quartz grains (Fig. 6f). The silica cement contents in Ti-3 sandstones are much less relative to those in the

**Table 5**

Statistics of minor and rare earth element contents of calcite cements. The REE values of seawater from Nothdurft et al. (2004) and those of river water from Goldstein and Jacobsen (1988) are also included.

Sample#		Fe (ppm)	Mn (ppm)	Sr (ppm)	Mn/Fe	La (ppb)	Ce (ppb)	Pr (ppb)	Nd (ppb)	Sm (ppb)	Eu (ppb)	Gd (ppb)	Tb (ppb)	Dy (ppb)	Ho (ppb)	Er (ppb)	Tm (ppb)	Yb (ppb)	Lu (ppb)	$\Sigma$ REE (ppm)	Ce/Ce*
3344.6	n	11	5	5	5	6	6		6	6	6			6	6	6	6	6	6	6	
	Mean	134	651	653	5.5	3411	6387		3447	869	310			494	140	119	15	0.86			
	S.D.	117	88	257	3.5	1485	2237		885	269	73			141	91	39	5	0.05			
	Max	397	819	1114	10.6	5818	10296		4945	1208	426			630	289	192	24	0.93			
	Min	37	569	444	1.6	1874	3382		2050	546	183			257	30	64	8	0.79			
3367.8	n	11	4	4	4	7	7		7	7	7			7	7	7	7	7	7	7	
	Mean	40	338	1725	7.9	520	1359		994	315	70			114	26	27	4	0.90			
	S.D.	9	31	60	1.9	219	296		148	64	19			24	16	15	0.5	0.11			
	Max	58	374	1759	11.1	885	1942		1183	378	104			141	50	45	5	0.09			
	Min	28	295	1621	6.2	249	1015		750	176	44			77	6	5	3	0.78			
3371.1	n	13	5	5	5	13	13		13	13	13			13	13	13	13	13	13	13	
	Mean	120	222	1145	1.6	2881	5644		3234	962	273			526	202	199	14	0.86			
	S.D.	58	29	623	0.6	2837	6158		2998	913	251			549	201	223	14	0.18			
	Max	225	243	2260	2.5	8941	18967		9997	2877	798			1642	600	693	44	0.90			
	Min	44	181	640	0.8	346	669		549	227	49			98	38	36	2	0.71			
3379.1	n	16	6	6	6	10	10		10	10	10			10	10	10	10	10	10	10	
	Mean	225	61	1572	0.4	1158	2230		1576	604	167			241	119	79	6	0.78			
	S.D.	126	8	549	0.2	695	1059		662	318	117			107	151	44	3	0.07			
	Max	494	77	1964	0.6	3027	4689		2784	1297	491			470	538	152	12	0.95			
	Min	70	54	446	0.2	433	889		825	227	75			115	14	21	3	0.38			
3386.5	n	10	4	4	4	8	8		8	8	8			8	8	8	8	8	8	8	
	Mean	60	1527	1436	22.4	1229	2389		1443	481	166			295	130	163	6	0.84			
	S.D.	28	296	627	10.2	1573	3220		1985	646	201			369	128	171	10	0.10			
	Max	127	1769	2218	36.4	5155	10358		6464	2019	601			1072	375	453	26	0.98			
	Min	34	1022	676	8.1	124	211		81	24	29			17	17	36	1	0.76			
Seawater	Value					691	787	118	479	96	22	122	19	125	30	90	77	12	3	0.59	
River water	Value (ppm)					39.6	80.9		36.4	6.9	1.4	5.3		4.2	2.0		1.7	0.3	179	0.97	

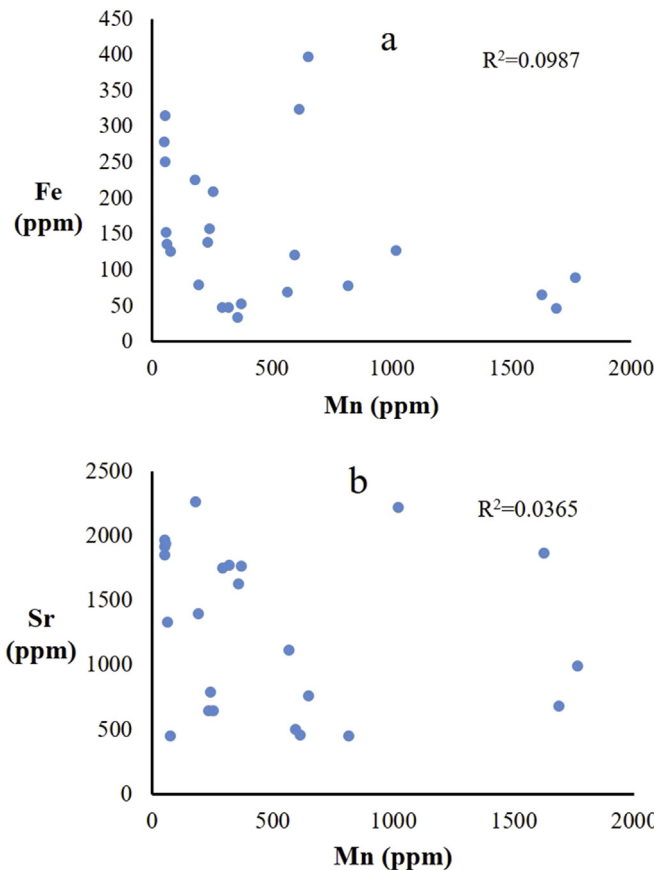


**Fig. 9.** Scatter diagrams of (a) Mn vs. Fe and (b) Mn vs. Sr for calcite cements.

clastic reservoirs of the Hibernia field of the Jeanne d'Arc Basin (4.3%–7.3%; [Brown et al., 1989](#); [Hesse and Abid, 1998](#)). The quartz overgrowths are more abundant in the sandstone intervals with poor calcite cements ([Appendix I](#)). Nonetheless, it is likely difficult to identify authigenic quartz overgrowths due to etched and partially replaced grain boundaries.

#### 4.4. Pyrite cement

Authigenic pyrite occurs in two occurrence forms, euhedral to subehedral microcubes replacing bioclasts and fine crystalline occluding intergranular pores and replacing remnants of calcite cements ([Figs. 5f and 6e](#)).

#### 4.5. Fluid inclusions microthermometry of calcite cements

Due to the scarcity of dolomite and siderite cements, the microthermometric and geochemical analyses are focused on the calcite cement.

The calcite cements in the Ti-3 sandstones host primary fluid inclusions including common mono-phase (all-liquid) fluid inclusions in the cores of calcite crystals, but rare two-phase (liquid and vapor) fluid inclusions generally in the rims of those crystals and in the fracture-filling calcites ([Fig. 7](#)). [Table 3](#) summarizes the results and statistics of microthermometric measurements. All-fluid inclusions size varies from 5 to 12  $\mu\text{m}$  and the two-phase fluid inclusions are <10  $\mu\text{m}$  with approximate liquid: vapor ratios of 6:1. Microthermometric measurements of homogenization temperature ( $T_h$ ), initial melting temperature ( $T_i$ ) and final ice-melting temperature ( $T_m$ ) were obtained from primary two-phase fluid inclusions. Measurements of  $T_i$  and  $T_m$  were also performed on several monophase aqueous inclusions. Since freezing alters the fluid inclusion's morphology, homogenization temperatures of the two-phase inclusions were measured first ([Lawler and Crawford, 1983](#)). The estimated salinities were calculated based on  $T_m$

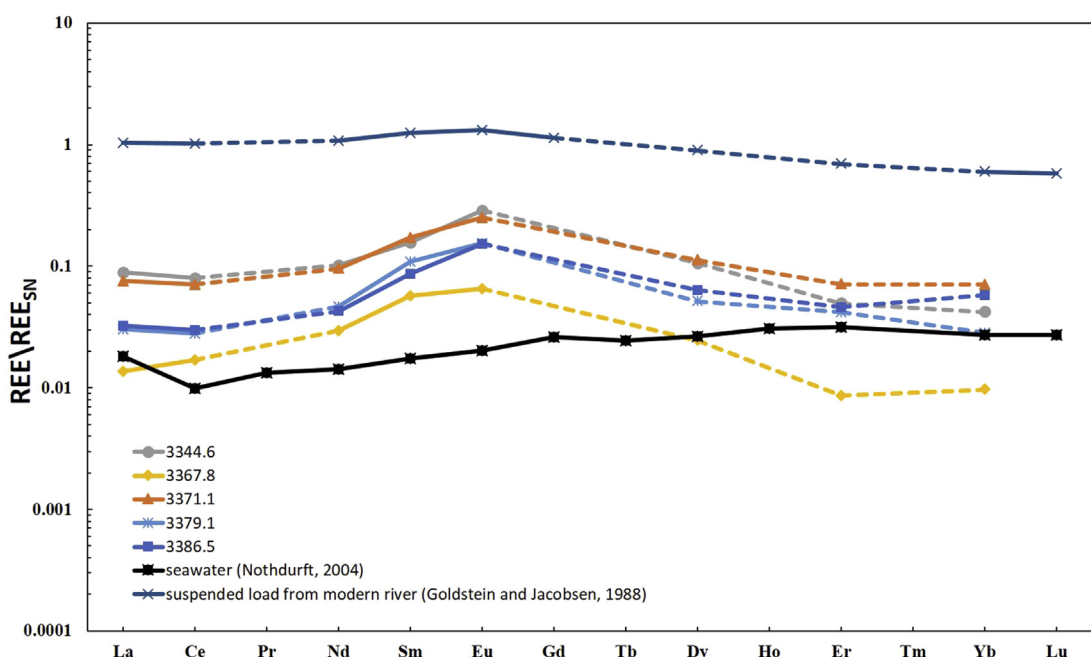


**Fig. 10.** Shale-normalized (PAAS) REE patterns of calcite cements (REE<sub>SN</sub>) in the Ti-3 sandstones, Lennard Shelf cements reflecting seawater-like pattern ([Nothdurft et al., 2004](#)) and suspended load from modern river water reflecting fluvial input pattern ([Goldstein and Jacobsen, 1988](#)). The Ce anomaly ( $\text{Ce}/\text{Ce}^*$ ) values were calculated based on the equation  $\text{Ce}/\text{Ce}^* = 3(\text{Ce}/\text{Ce}_{\text{shale}})/[(2\text{La}/\text{La}_{\text{shale}}) + (\text{Nd}/\text{Nd}_{\text{shale}})]$  of [de Baar et al. \(1985\)](#).

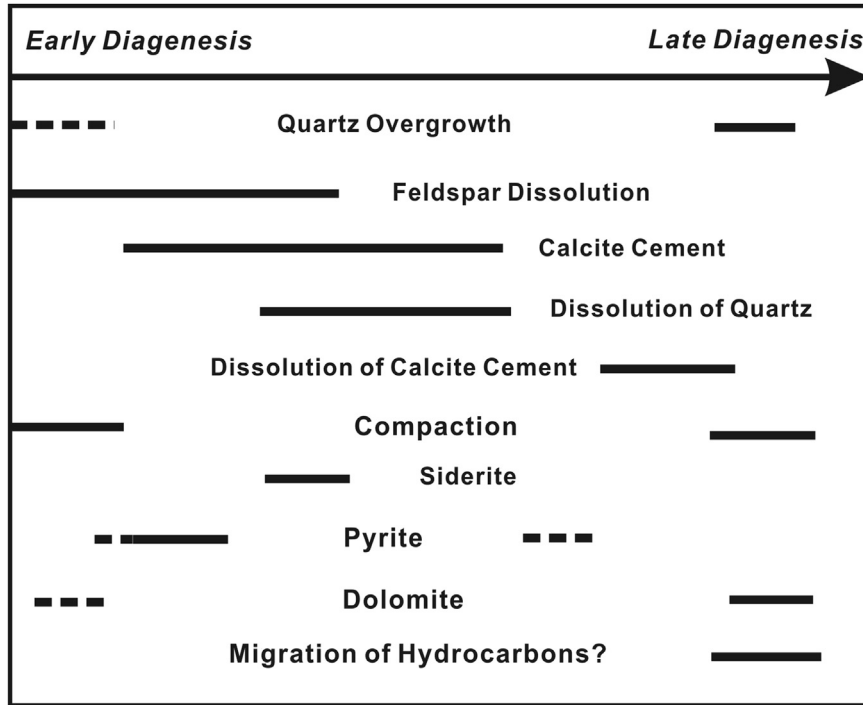


**Fig. 11.** Paragenetic sequence of the Ti-3 sandstones of the Bodhrán Formation based on petrographic relationships.

results (Bodnar, 2003).

The values of  $T_h$  for two-phase fluid inclusions in the intergranular calcite cements range from 63.9 to 83.1 °C ( $72.3 \pm 5.4$  °C,  $n = 27$ ; Table 3); however, those of the fracture-filling calcites are much higher ( $101.0 \pm 21.5$  °C,  $n = 16$ ; Table 3). The estimated mean salinities for intergranular and fracture-filling calcite cements are  $8.8 \pm 1.2$  eq. wt.% NaCl,  $n = 13$  and  $10.0 \pm 1.8$  eq. wt.% NaCl,  $n = 8$ , respectively (Table 3), whereas all-fluid inclusion have a lower salinity ( $3.0 \pm 1.7$  eq. wt.% NaCl,  $n = 28$ ; Table 3). All  $T_i$  values of two-phase inclusions from both types of calcites fall within the range between  $-45$  °C and  $-50$  °C (Appendix II).

#### 4.6. Fluid-inclusion gas ratios of calcite cements

The geochemistry and origin of diagenetic fluids can be better understood by combining results with those from fluid inclusion gas analysis (Blamey, 2012; Azmy and Blamey, 2013; Blamey et al., 2014). Six samples with high calcite cementation (>30%) were selected for fluid-inclusion gas analysis in the current study (Table 4, Appendix III). Five samples show a relatively similar weighted mean ratio of  $\text{CO}_2/\text{CH}_4$  and  $\text{N}_2/\text{Ar}$ , ranging from 1.04 to 2.47, 51.7 to 73.1, respectively; while one sample (#3334.8) has lower weighted mean ratio of  $\text{CO}_2/\text{CH}_4$  (0.57) and higher  $\text{N}_2/\text{Ar}$  (94.2). In case crushing liberates quartz-hosted inclusions, quartz fluid inclusion gas weighted mean data (Blamey et al., 2014) are listed in Table 4. The quartz inclusion analysis shows a remarkably distinct high weight mean ratio of  $\text{CO}_2/\text{CH}_4$  (96.8) compared with those from calcite cements.

#### 4.7. Carbon and oxygen isotopes

The C- and O- isotopic measurements of the intergranular calcite cements in the Ti-3 Member sandstones of the Bodhrán Formation (Fig. 8 and Table 2) show that the  $\delta^{13}\text{C}$  values have a slightly broad range of  $-4.8$  to  $-0.1\text{\textperthousand}$  VPDB (mean  $-2.9\text{\textperthousand} \pm 1.32\text{\textperthousand}$ ,

VPDB,  $n = 23$ ). The  $\delta^{18}\text{O}$  isotopic values cluster around  $-8\text{\textperthousand}$  VPDB, ranging from  $-11.0$  to  $-5.3\text{\textperthousand}$  VPDB (mean  $-8.3\text{\textperthousand} \pm 1.23\text{\textperthousand}$  VPDB,  $n = 23$ ). The mean  $\delta^{13}\text{C}$  and  $\delta^{18}\text{O}$  values of the fracture-filling calcites are  $-2.0\text{\textperthousand} \pm 0.2\text{\textperthousand}$  VPDB,  $n = 3$  and  $-10.8\text{\textperthousand} \pm 0.1\text{\textperthousand}$  VPDB,  $n = 3$ , respectively.

#### 4.8. Minor and rare earth elements analysis

The concentrations of minor elements (e.g., Fe, Mn, Sr) and rare earth element (REE) in calcite cements were analyzed by SIMS (Table 5, Appendix IV). The contents of Mn vary from 54 to 1527 ppm with a mean value of  $508 \pm 515$  ppm and those of Fe range from 28 to 494 ppm with a mean value of  $126 \pm 110$  ppm. In the analyzed samples, contents of Mn are higher than those of Fe except for only one sample (# 3379.1; Table 5). The Sr mean concentrations show a relatively narrower range of variations (from 1145 to 1725 ppm; Table 5) except for sample# 3344.6, which has considerably lower Sr (653 ppm). No significant correlation was found between Mn and Fe, or Mn and Sr (Fig. 9).

The mean total REE ( $\sum\text{REE}$ ) values of investigated calcite cements vary from  $4 \pm 0.5$  ( $n = 7$ ) to  $15 \pm 5$  ppm ( $n = 6$ ) (Table 5). The mean Ce anomaly values (de Baar et al., 1985) display a narrow range and are close to unity (Table 5). The shale normalized REE distribution patterns (relative to PAAS) of calcite cements (REE<sub>SN</sub>) are generally consistent, exhibiting the same medium REEs-enrichment and slight heavy REEs-depletion (Fig. 10).

## 5. Discussion

### 5.1. Diagenesis and paragenetic sequence

Fig. 11 summarizes the paragenetic sequence for the Ti-3 sandstones based on petrographic relationships. The current compositions of sandstones are likely altered relative to those at the time of deposition due to diagenetic processes (e.g. Brown et al.,

1989). The general paragenetic sequence of sandstones inferred from petrographic examination is as follow: (1) unstable minerals leaching by meteoric waters, (2) pervasive precipitation of calcite cements along with early pyrite, (3) corrosion of quartz grains followed by precipitation of siderite, (4) major calcite cement dissolution due to migration of hydrocarbon, and (5) precipitation of dolomite and late pyrite.

### 5.1.1. Quartz overgrowth

Minor quartz grains with quartz overgrowths were enclosed by poikilotopic calcite cements (Fig. 6b), which indicates that some overgrowths predated massive calcite cementation and that these overgrowths are inherited since the Flemish Pass sandstones are possibly derived from reworked sediments particularly when the overgrowths are scarce and have abraded morphology (e.g., Hutcheon et al., 1985; Lowe et al., 2011). The infrequent occurrence of quartz overgrowths in pervasive calcite cemented intervals suggests that the precipitation of early calcite might have inhibited quartz from forming syntaxial overgrowths. However, some quartz cements might also occur at the late diagenetic stage after calcite dissolution as indicated by the clean-edge texture of some overgrowths and the absence of poikilotopic calcite around them. Sutured grain-grain contacts are very rare in the Ti-3 sandstones and thus the extra silica unlikely originated from pressure solution but provided by fluids released from adjacent silty mudstone beddings in the sequence by mechanical compaction (e.g., McBride, 1989) or in-situ dissolution of feldspars (e.g., Walderhaug, 1990; Worden and Morad, 2000). In addition, silica released from local

dissolution of quartz and/or mica is possibly another supply (e.g., Walker, 1960; McBride, 1989).

### 5.1.2. Quartz grain corrosion

The quartz grains exhibit dissolution textures in association with poikilotopic calcite precipitation. They are characterized by irregular pitted, corroded boundaries and embayment margins in the thin sections (Fig. 5a). This process occurs alkaline conditions, which suit for calcite precipitation (e.g., Epstein and Friedman, 1982; Normore, 2006; Zaid and Gahtani, 2015). Earlier studies of the same feature (Friedman et al., 1976; Bennett and Siegel, 1987; Gorbushina and Palinska, 1999) suggested that the increased pH produced by biological activities facilitate the dissolution of silica and silicate minerals (e.g., quartz, feldspar). Thus, co-occurring algae in the Ti-3 sandstones probably contributed to quartz corrosion since the photosynthesis by algae might have enhanced the alkaline conditions as well as super-saturated fluids with respect to calcite (e.g., Friedman et al., 1976; Epstein and Friedman, 1982; Brehm et al., 2005). The quartz deposited in shallow marine sediments exhibits the same corrosion textures similar to those formed in the lab condition by biofilm growth (Brehm et al., 2005), which supports that microbial activities are capable of quartz breakdown. However, high alkaline environment is not common in nature and quartz dissolution could be therefore carried out by causes other than pH variations such as the crystallography and free energy of the quartz grains, which can be a potential sub-factor contributing to the extent of dissolution (Burley and Kantorowicz, 1986).

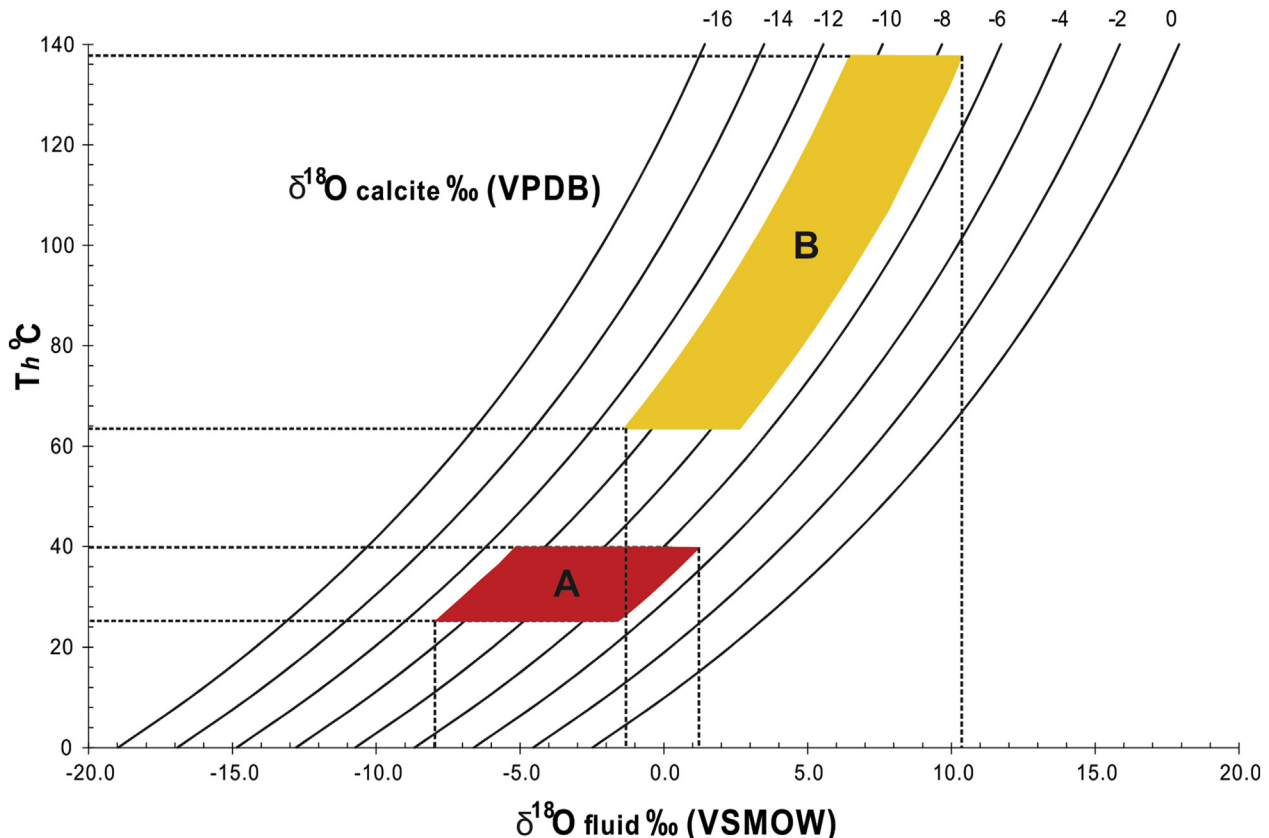


**Fig. 12.** Temperature ( $T$ ) vs.  $\delta^{18}\text{O}_{\text{fluid}}$  for various  $\delta^{18}\text{O}_{\text{calcite}}$  values that were reconstructed from the following equation:  $10^3 \ln a_{(\text{calcite-water})} = 2.78 \times 10^6 T^{-2} - 2.89$  (Friedman and O'Neil, 1977). The vertical bars indicate the  $\delta^{18}\text{O}_{\text{fluid}}$  compositions based on the ranges of  $\delta^{18}\text{O}_{\text{calcite}}$  values and homogenization Temperature ( $T_h$ ) of each identified calcite cement phase. Details in text. Field A refers to the early intergranular poikilotopic calcite and B to the late and fracture-filling calcite.

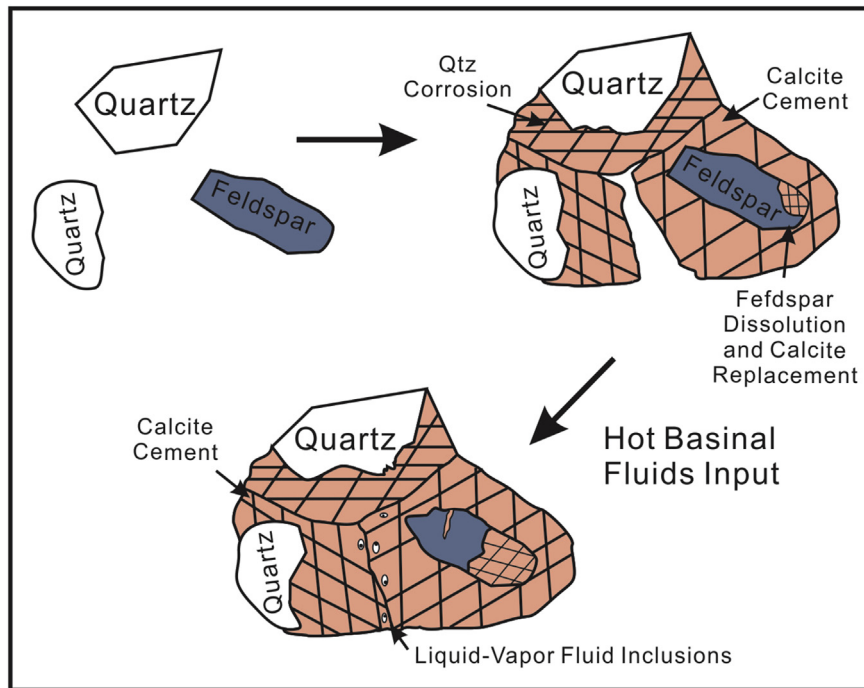


**Fig. 13.** Schematic diagram summarizes the stages of formation of fluid inclusions in the calcite cements of the investigated sandstones. All-liquid fluid inclusions occur in the cores of poikilotopic calcite that precipitated at shallow burial, while liquid–vapor fluid inclusions form later in the crystal rims with progressive burial.

### 5.1.3. Calcite cementation

Petrographic examination suggests that the poikilotopic calcite was precipitated during early diagenesis, which is inferred by high intergranular volume (IGV; Table 2), commonly well-preserved bioclasts, and loosely compacted framework grains with “floating” texture (Fig. 5a, d, Loucks et al., 1977; Hesse and Abid, 1998; Wanas, 2008; Liu et al., 2014; Nyman et al., 2014). The continuous twinning planes passing through sediment grains (Fig. 6a) suggest that the cement engulfed those grains before subsequent diagenesis (Blamey et al., 2014). Fracture-filling calcite likely developed during late burial, which is indicated by the sharp cut and clear boundaries of the fracture through sediments (Fig. 6d). Minor bluish fluorescent spots can be traced in the calcite cements under ultraviolet light (Fig. 6g), which refers to the early emplacement of hydrocarbon along with calcite precipitation (e.g., Parnell et al., 2001).

### 5.1.4. Precipitation of other authigenic minerals

The dolomite was precipitated after calcite dissolution, which is indicated by its occurrence in the sandstones out of extensive calcite cements and filling in enlarged pores.

The spherulitic siderite is one of the early cements. It followed calcite cementation occurring along the quartz embayment (Fig. 6b). The dull CL of samples having both calcite and siderite (Fig. 6c) indicates precipitation from Fe-rich pore water.

Pyrite occurs as early and late cement in the Ti-3 sandstones. Early pyrite occurs in the extensive calcite-cemented interval (e.g., Brown et al., 1989; Hesse and Abid, 1998), whereas, late pyrite fills secondary pores which suggests that it formed after the dissolution of calcite.

### 5.1.5. Albition of K-Feldspars

Petrographic examinations reveal partial albited K-feldspars engulfed by early poikilotopic calcite cements (Fig. 5g). However, the albition of K-feldspar appears more likely at greater burial

with higher temperature after mesodiagenesis (Morad et al., 1990; Baccar et al., 1993; González-Acebrón et al., 2010). The observed albitization in the Ti-3 sandstones might therefore be provenance related, and inherited from the source rocks particularly when the maximum  $T_h$  of the poikilotopic calcite (83.1 °C; Table 3) is similar to the threshold temperature for albitization (83 °C; González-Acebrón et al., 2010).

### 5.1.6. Dissolution

The investigated sandstones experienced two main episodes of dissolution during diagenesis. Petrographic examinations suggest that minor partially-dissolved feldspar grains occurring in the poikilotopic calcite cement support a scenario of early dissolution by meteoric water leaching. The albited K-feldspars retain skeletal textures, suggesting that the leaching probably started on replaced cleavage planes (Fig. 6f). Thus, original Ti-3 sandstones contained more feldspars. A major calcite cement dissolution occurred during progressive burial by acidic basinal fluids, which is evident from the abundant irregular secondary pores and remnants of calcite cement crystals (Fig. 5b, f and Fig. 6e). Furthermore, the pitted quartz grains in the cemented intervals also indicates that the former calcite cement has been dissolved. This large-scale dissolution also affected framework grains and accessory minerals and, therefore, altered original composition of the sandstones. It suggests that maturation of organic matters (e.g., hydrocarbon and coals) was responsible for the acidic diagenetic fluids (e.g., Brown et al., 1989; Taylor et al., 2000; Normore, 2006; Dutton, 2008). This late stage calcite dissolution significantly improved porosity and permeability in the investigated sandstones.

### 5.1.7. Compaction

Although the early calcite cement has to some extent retarded mechanical compaction by the overlying sediment loads, micro-cracks still occurred in some detrital quartz (Fig. 6h). Minor quartz grains are fractured, and enclosed by poikilotopic calcite (Fig. 6h).

This suggests that the early calcite cementation formed during shallow to middle burial. In some uncemented intervals, a few quartz grains exhibit concavo-convex contacts (Fig. 6f), which is consistent with the expected continuous compaction with progressive burial after major calcite dissolution.

## 5.2. Origin of calcite cement

This early poikilotopic calcite has been also documented and studied by Hutcheon et al. (1985), Brown et al. (1989), Hesse and Abid (1998), and Liu et al. (2014). It may result also from the recrystallization of micritic cements (Saigal and Bjørlykke, 1987). The abundant bioclasts (Appendix I) are more likely the source for calcite cements (e.g., Bjørkum and Walderhaug, 1990; McBride et al., 1995). An earlier previous sedimentological study (Haynes et al., 2013) suggested that the sediments were likely deposited in a transgressive system that has been exposed to meteoric influence. When depositional environment shifts from braided fluvial upward to restricted nearshore marine, the rate of deposition became slower. This prolonged subsidence enhanced calcite cement precipitation (Raiswell, 1987; Morad et al., 2010).

### 5.2.1. Oxygen and carbon isotopes

The oxygen isotopic compositions for intergranular calcite cements ( $-11.0$  to  $-5.3\text{\textperthousand}$  VPDB) are significantly lower than the composition of the best preserved Tithonian marine carbonates ( $-1.5$  to  $-0.5\text{\textperthousand}$  VPDB; Veizer et al., 1999). Mozley and Burns (1993) suggested that mixing marine water with meteoric water might account for a similar depletion of  $\delta^{18}\text{O}$  values in an offshore environment (e.g., Land, 1995; Hutcheon et al., 1985; Scotchman, 1991). This implies that the calcite cement in the Ti-3 sandstones precipitated from modified marine waters in most likely a fluvio-shallow marine environment (e.g., Hesse and Abid, 1998; Haynes et al., 2013). However, the  $\delta^{18}\text{O}$  values of fracture-filling calcites tend to be more depleted relative to their intergranular counterparts (Fig. 8). This implies that they formed in later burial setting of higher temperature, which is consistent with their petrographic features. Very few  $\delta^{18}\text{O}$  values of intergranular calcite are depleted as those of the fracture-filling one indicates that poikilotopic calcite continuously precipitated during the progressive burial.

The occurrence of all-liquid fluid inclusions particularly in the core of intergranular calcite cement crystals suggests that they

mainly precipitated at near surface temperature possibly between 25 and 40 °C (Goldstein and Reynolds, 1994; Hesse and Abid, 1998; Azomani et al., 2013; Nyman et al., 2014). However, the crystals grew with progressive burial as indicated by the entrapment of primary two-phase fluid inclusions along the rims of some of those crystals. Therefore, estimates of the oxygen isotopic composition of the parent fluids of the calcite cements can be calculated (Friedman and O'Neil, 1977). Fig. 12 demonstrates the calcite–water equilibrium relationship based on temperature. The measured  $\delta^{18}\text{O}$  of the early calcite cements and their suggested approximate temperature of precipitation (25–40 °C) imply that the  $\delta^{18}\text{O}$  values of their parent diagenetic fluids were approximately between  $-8$  and  $1.1\text{\textperthousand}$  VSMOW (Fig. 12). Clark and Fritz (1997) suggested that the average  $\delta^{18}\text{O}$  value of present-day meteoric waters is  $\sim 4\text{\textperthousand}$  VSMOW lower than that of modern tropical seawater. Assuming that this difference was consistent during the Jurassic times, the  $\delta^{18}\text{O}$  values of Jurassic meteoric waters would be  $-5$  to  $-4\text{\textperthousand}$  VSMOW since the  $\delta^{18}\text{O}$  values of Jurassic marine water ranged from  $-1$  to  $0\text{\textperthousand}$  VSMOW (Veizer et al., 1999; Holmden and Hudson, 2003). Thus, the estimated  $\delta^{18}\text{O}$  values of diagenetic fluids generally fall within the range between the values of the Jurassic marine water. Calculated low salinity estimates for all-liquid fluid inclusions (Table 3; 3.5 eq. wt.% NaCl for modern sea water salinity) also support the precipitation from a mixture of marine and meteoric waters, which is also consistent with sediments' fluvio-estuarine depositional facies (Haynes et al., 2013). However, the  $\delta^{18}\text{O}$  and  $T_h$  values of the calcite cements with primary two-phase fluid inclusions (fracture-filling and crystal rims of intergranular) reflect hydrothermal  $^{18}\text{O}$ -enriched parent fluids ( $-1.2$  to  $+10.3\text{\textperthousand}$  VSMOW; Fig. 12), which is expected for circulated hot basinal fluids of relatively deeper burial settings (e.g., Azmy et al., 2009; Concliffe et al., 2010; Azomani et al., 2013; Olanipekun et al., 2014). This is also consistent with the fracture-filling calcite that yields even higher  $T_h$  values and salinities estimates (Table 3). In summary, the  $\delta^{18}\text{O}$  composition of the intergranular and deep burial fracture-filling calcite cements suggest that they primarily precipitated from mixed marine and meteoric waters that became hotter and more  $^{18}\text{O}$ -enriched with progressive

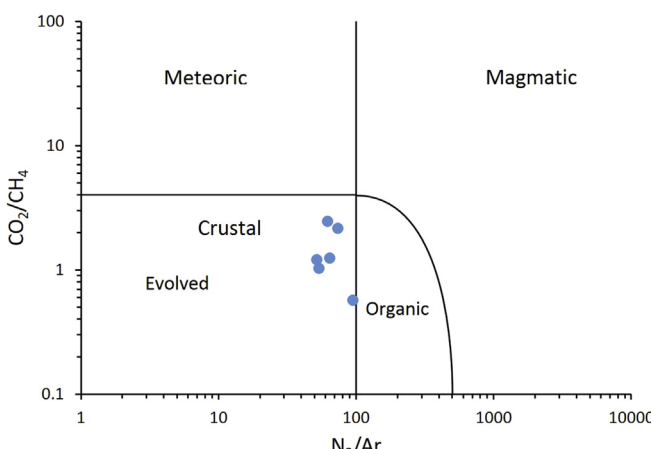


**Fig. 14.** Plot of  $\text{CO}_2/\text{CH}_4$  vs.  $\text{N}_2/\text{Ar}$  for gas-inclusion analyses of the intergranular calcite cements from the Ti-3 sandstones (modified from Norman and Moore, 1999).

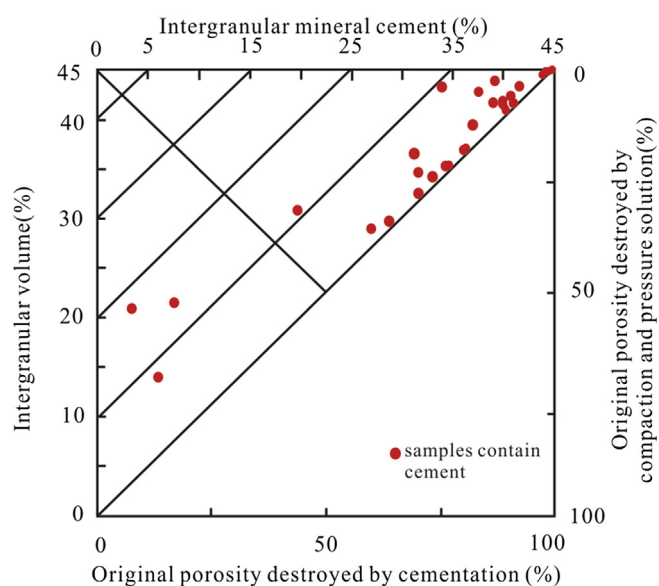


**Fig. 15.** Diagram showing the intergranular volume vs. calcite cement volume in the Ti-3 sandstones, modified from Lundegard (1992).

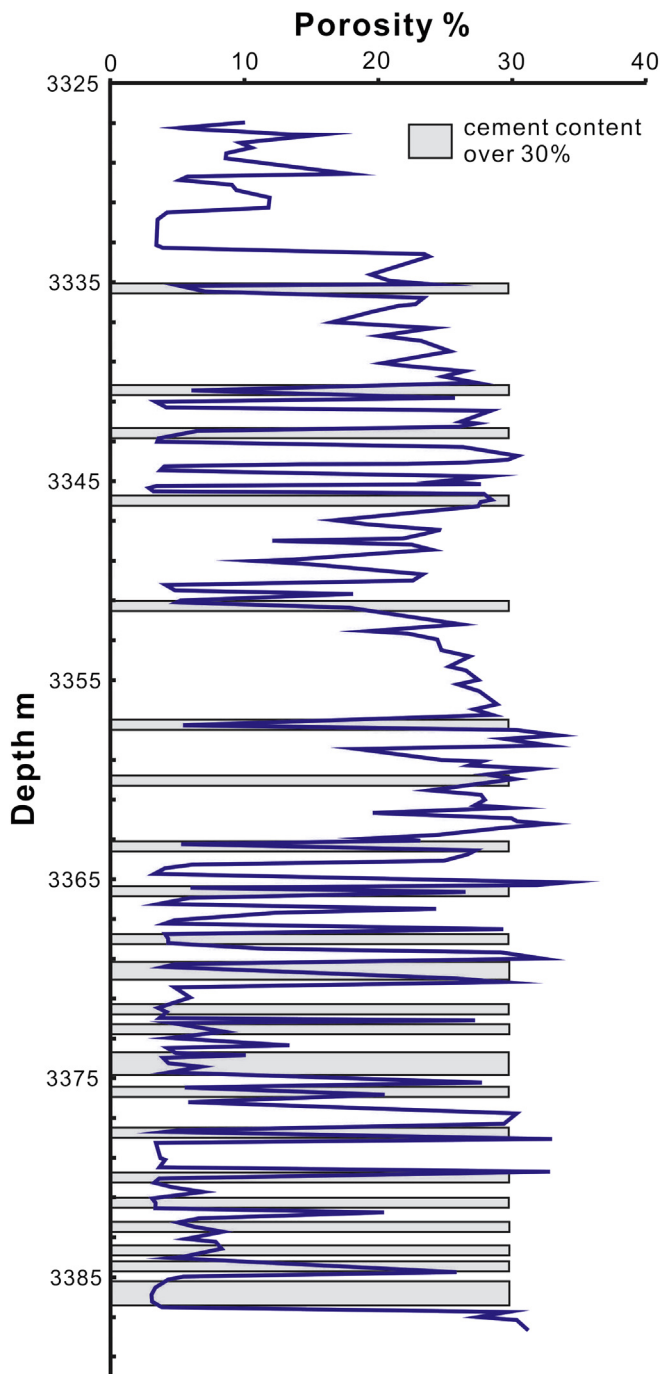


**Fig. 16.** Diagram showing the relationship between porosity distribution in sandstones intervals and calcite-cemented zones. The gray bar represents intervals with calcite cements over 30%. The porosity data are acquired from Natural Resources Canada website ([http://basin.gdr.nrcan.gc.ca/index\\_e.php](http://basin.gdr.nrcan.gc.ca/index_e.php)).

burial and circulation in the basin. Based on petrographic observations and stable isotope conclusions, Fig. 13 shows a brief sketch that summarizes the stages of fluid inclusions formation in the investigated cements.

Biogenic carbonates are one of major sources for carbonate cements in sandstones or mudstones since the Upper Jurassic sandstones often contain plentiful calcite cements that were mainly sourced from calcareous organisms on the sea-floor (e.g., Bjørlykke and Jahren, 2010). The carbon isotopic values of the currently

investigated calcites range between  $-4.8$  and  $-0.1\text{‰}$  VPDB, which imply that they were originated mostly from seawater and dissolution of bioclasts (e.g. Hesse and Abid, 1998; Wanas, 2008; Dutton et al., 2012; Nyman et al., 2014). The decarboxylation of organic matter during early burial stage releases light ( $^{12}\text{C}$ -riched)  $\text{CO}_2$ , which explains some of the slightly low  $\delta^{13}\text{C}$  values of the Ti-3 sandstones calcites (Fig. 8; Irwin et al., 1977; Morad, 1998; Faure and Mensing, 2005). The abundance of bioclasts within the Ti-3 sandstones provides a solid evidence for a biogenic origin of calcite cements. In addition, calcareous siltstones adjacent to the Ti-3 sandstones (Fig. 3) may provide additional external sources for the calcite via pore fluids expelled by compaction (e.g. Dutton et al., 2000; McBride et al., 1995).

### 5.2.2. Minor and rare earth elements

It is well-known that Fe and Mn concentrations are the major factor controlling the luminescent degree in diagenetic calcites (Barnaby and Rimstidt, 1989). Since Mn has been identified as the main activator while Fe as the quencher of luminescence, the intensity of CL is mainly controlled by the Mn/Fe ratio of calcite (Heydari and Moore, 1993). Generally, calcite with  $\text{Mn} > \text{Fe}$  exhibits brighter luminescence and vice versa (Machel et al., 1991). On the other hand, Mn and Fe contents associated with calcite luminescence reflect the redox conditions during cement precipitation (e.g., Frank et al., 1982; Barnaby and Rimstidt, 1989). The Mn contents of the intergranular calcite are commonly more enriched than Fe (Table 5), which is consistent with their dull/moderate to bright CL images. This implies that early-burial calcite cements with dull CL likely precipitated in shallow-burial and less reducing environment but those which exhibit bright CL reflect the late burial settings (Fig. 5d). The Sr contents of the intergranular calcite cement are high (from 653 to 1725 ppm), and reflect influence of marine water (Banner, 1995; Taylor et al., 2000). High Sr concentrations ( $>1000$  ppm) also suggest that calcite cement could be sourced from dissolution of aragonitic shells (e.g., Kinsman, 1969; Hutcheon et al., 1985; Dickson, 1990; Thomas et al., 2004).

Rare earth elements (REE) consist of fifteen lanthanide ions (from La to Lu) and have a relatively short oceanic residence time (less than  $10^3$  yrs; Alibo and Nozaki, 1999). Due to their respectively narrow range of partition coefficient values in calcites, variations in series can record the chemical changes of fluid input (Zhong and Mucci, 1995), therefore reflect the nature of ambient fluids when carbonates precipitated. All REE are naturally trivalent except for Cerium (Ce) and Europium (Eu) ( $\text{Ce}^{4+}$  and  $\text{Eu}^{2+}$ , respectively); hence the systematic change of Ce and Eu can offer further information in redox conditions (Sholkovitz et al., 1994; Zhong and Mucci, 1995).

The  $\text{REE}_{\text{SN}}$  patterns of the currently investigated calcites from various depths of the studied borehole exhibit similar and almost parallel profiles (Fig. 10). Combined with the stable isotope and fluid inclusion results, the REE results confirm that the calcite cements in the Ti-3 sandstones precipitated from the same parent diagenetic fluids that were circulated through the basin during burial. The  $\text{REE}_{\text{SN}}$  patterns of the investigated cements generally exhibits light negative Ce anomalies and positive Eu anomalies (Fig. 10). They are not parallel to the typical seawater profile characterized by a remarkable negative Ce anomaly and depleted LREE (light REE, La to Nd) relative to HREE (heavy REE, Ho to Lu) (Fig. 10; e.g. Elderfield and Greaves, 1982; Bau and Dulski, 1996; Nothdurft et al., 2004; Azmy et al., 2011), but similar to river–water profile with MREE enrichment (medium REE, Sm to Dy) (Fig. 10; Goldstein and Jacobsen, 1988). The scenario of Ce anomaly caused by removal of Ce by Fe-hydroxides to be enriched in chlorite and sphene (e.g., Blamey et al., 2014) is unlikely, because those minerals are very rare in the Ti-3

sandstones. Alternatively, the Ce anomaly occurs in shallow seawater environment due to oxidation of soluble  $\text{Ce}^{3+}$  to insoluble  $\text{Ce}^{4+}$  through bacterial mediation (Elderfield and Greaves, 1982; German and Elderfield, 1990; Alibo and Nozaki, 1999). Thus, the Ce anomaly reflects the influence of contribution of marine water to the parent diagenetic fluids, which is consistent with the fluvio-estuarine sedimentary environment (Haynes et al., 2013) and also agrees with the suggestion of mixed meteoric and seawaters origin for the diagenetic fluids. In addition, the calculated Ce anomaly values (Table 5) confirm that less soluble  $\text{Ce}^{3+}$  existed in the diagenetic fluids at that period, which suggests a suboxic condition during precipitation of calcites (e.g., de Baar et al., 1988; Azomani et al., 2013). Positive Eu anomaly has been documented by earlier studies in fluids from hydrothermal vents at the seafloor and their associated carbonates (e.g., Elderfield and Greaves, 1982; Hongo and Nozaki, 2001; Bau et al., 2010). Also, Sverjensky (1984) and Bau et al. (2010) proposed that divalent europium ( $\text{Eu}^{2+}$ ) is dominant in marine hydrothermal fluids. Thus, the positive Eu anomaly (Fig. 10) reflects the contribution from the dissolution of plagioclase in sandstones by diagenetic fluids during burial (Lee et al., 2003; Bau et al., 2010).

### 5.2.3. Fluid-inclusion gas ratios in calcite cements

Ratios of gases trapped in the fluid inclusions have been utilized to shed the light on the origin of fluid sources in diagenetic environments (e.g. Blamey, 2012; Azmy and Balmey, 2013; Azomani et al., 2013; Olanipekun et al., 2014). The  $\text{CO}_2/\text{CH}_4$  versus  $\text{N}_2/\text{Ar}$  diagram, improved by Norman and Moore (1999), is an effective tool to differentiate between fluid sources by classifying data into three general zones: meteoric, crustal (basinal) and magmatic fluids. A field labeled the “organic” was introduced to the crustal area when Norman and Moore (1999) proved that excess nitrogen will be yielded in certain geothermal systems.

The  $\text{CO}_2/\text{CH}_4$  and  $\text{N}_2/\text{Ar}$  ratios of the calcite cements in the Ti-3 sandstones are presented in Fig. 14, showing that all data are well constrained in the crustal zone. This suggests that calcite cements originated from crustal (basinal) fluids, i.e. modified marine fluids, which is consistent with the conclusions from stable isotopes, minor and trace elements, fluid-inclusion studies and petrography. However, one of the samples has a higher  $\text{N}_2/\text{Ar}$  ratio that plots nearly at the boundary of the “organic” field (Fig. 14, Table 4), which implies that the disintegration of some organic matter might have released some extra  $\text{N}_2$  that contributed to the ratio (Norman and Moore, 1999; Azmy and Blamey, 2013). This is consistent with the correlated low  $\text{CO}_2/\text{CH}_4$  of the same sample since  $\text{N}_2$  and  $\text{CH}_4$  are by products of protein decay particularly in the late stages of diagenesis (Norman and Moore, 1997, 1999; Azomani et al., 2013; Azmy and Blamey, 2013).

### 5.3. Impact on sandstone porosity

Calcite cementation has been the focus of reservoir studies because it significantly influences the reservoir quality (e.g., Saigal and Bjørlykke, 1987; Bjørlykke et al., 1989; Taylor, 1990; Dutton et al., 2000; Longstaffe et al., 2003; Nyman et al., 2014; Liu et al., 2014). In the Ti-3 sandstones, over 75% original porosity loss was primarily due to calcite cementation (Fig. 15). A negative correlation between calcite cement contents and porosity suggests that pervasive calcite cementation was the dominant diagenetic mineral affecting porosity reduction (Fig. 16).

On the contrary, the early precipitated calcite cement leads to rigid framework, and retards the adverse impact by overburden compaction. However, secondary pores developed and throats reopened by calcite dissolution, which was a key process to improve

reservoir quality after deep burial. In the high porosity sandstone intervals, pores are mainly secondary in origin. Successive high porosity horizons are generally underlying silty mudstone beds with coal stringers (Figs. 3 and 16). Thus, the uncemented horizons may be the result of leaching process by organic acids released from coals (e.g. Percival, 1983; Van Keer et al., 1998; Taylor et al., 2000). The secondary porosity evolution is also related to the organic-acids produced from hydrocarbon maturation particularly when the Tithonian sandstones in the Flemish Pass Basin contain interbedded shales with 8%–12% TOC (Haynes et al., 2012). Thus, despite well-developed early calcite cementation, some Ti-3 sandstone intervals are porous and demonstrate a good reservoir quality.

Petrographic examination indicates that oil traces (Enachescu, 2014) exhibit signs of early emplacement of hydrocarbon. The microthermometric measurements of  $T_h$  (70–137 °C) provide values within the oil window (50–150 °C), which implies that oil migration might have occurred much earlier prior to diagenesis completion, and the Ti-3 sandstones could have been a hydrocarbon pathway (e.g. Parnell et al., 2001). The pervasive calcite cement brings important predictions in reservoir quality; however, in order to further understand the impacts of calcite cement on a basinal scale, modeling of calcite concretion distribution need to be extensively taken into account in future studies.

## 6. Conclusions

The Upper Jurassic Ti-3 sandstones of the Flemish Pass Basin consists of sublitharenites with high volumes of early burial pore-filling poikilotropic but minor late burial fracture-filling calcite cements, which their origin and geochemical compositions were controlled by the diagenetic environment and sediment compositions.

Microthermometric analyses ( $T_h$  and salinity estimates), along with petrographic examinations, suggest that the intergranular/poikilotropic calcite cements started precipitation during early burial but the fracture-filling calcite developed at deep burial settings, which is consistent with their stable isotope compositions.

The calculated estimates of the  $\delta^{18}\text{O}$  composition of parent diagenetic fluids, the fluid-inclusion gas ratios and Ce anomaly values suggest that the calcite cements precipitated from modified seawater that was mixed with meteoric water in suboxic conditions.

The high Sr contents also reflect some contributions from in-situ dissolution of bioclasts (possibly aragonitic shells) and positive Eu anomaly reflects contributions from the dissolution of plagioclase during diagenetic burial. The similarity in the REE<sub>SN</sub> patterns suggests that the cements developed from basinal fluids that their composition evolved through the circulation in the basin sediments.

Despite the early cementation of the Flemish Basin Ti-3 sandstones that blocked significant volume of the pore space, the acidic fluids generated by maturation of organic matter during burial resulted in significant dissolution of the calcite cements and the development of high secondary porosity of up to 28% in some horizons, particularly those associated with organic-rich silty mudstones beds.

## Acknowledgments

The authors gratefully thank the editor (Dr. Ihsan Al-Aasm) and the reviewers for their valuable comments. Also, special thanks to Mr. Glenn Piercy for operating the CREATI SIMS lab facilities on campus, and Dr. James Coniffe for providing constructive suggestions during the fluid inclusion analyses. This project was supported by funding (to Dr. Karem Azmy) from the Sucor-Mitacs Program.

## Appendix

### Appendix I

Mineralogic composition (%) and porosity (%) of Ti-3 reservoir sandstone determined by optical microscope.

Samples#	Ave. Grain size ( $\mu\text{m}$ )	Grain shape	Quartz* (%)	Feldspar* (%)	Lithic Fragment* (%)	Calcite Cement(%)	Pyrite(%)	Quart Overgrowth(%)	Bioclast(%)	Porosity(%)
3327.1	very-fined grain									
3329.4	very-fined grain									
3330.1	very-fined grain									
3331.7	very-fined grain									
3332.6	very-fined grain									
3332.7	very-fined grain									
3333.2	very-fined grain									
3334.4	very-fined grain									
3335.6	40	angular-subangular	90	3	7	45	5	3	7	1
3336.6	very-fined grain									
3337.1	very-fined grain									
3337.6	very-fined grain									
3339.3	170	subangular-subrounded	83	7	10	0	13	2	10	15
3340.6	110	subangular-subrounded	88	2	10	32	4	3	7	6
3341.9	140	subangular	87	3	10	0	2	4	7	18
3342.6	180	subangular	92	2	6	40	0	2	3	2
3343.6	140	angular-subangular	86	2	12	0	2	1	9	22
3344.6	150	angular-subangular	88	3	9	47	2	2	9	1
3344.6-2	160	angular-subangular	88	3	9	46	2	2	9	1
3345.8	very-fined grain									
3346.6	very-fined grain									
3348.6	90	angular-subangular	90	4	6	5	4	1	13	8
3350.2	very-fined grain									
3351.3	100	angular-subangular	92	2	6	36	1	2	8	1
3352.5	very-fined grain									
3354.2	150	subangular-subrounded	94	2	4	0	4	3	5	18
3355.6	150	angular-subangular	85	7	8	7	6	3	3	15
3356.4	180	subangular-subrounded	91	4	5	0	3	2	8	7
3357.2	130	angular-subangular	97	1	2	40	4	3	4	1
3357.7	200	subangular-subrounded	89	1	10	0	6	4	5	20
3360.4	110	angular-subangular	91	1	8	32	2	2	12	4
3361.1	160	angular-subangular	85	5	10	0	2	3	8	14
3362.6	130	subangular-subrounded	86	3	11	0	6	2	6	17
3361.6	180	subangular-subrounded	92	1	7	0	5	3	5	15
3363.4	100	angular-subangular	86	3	11	37	1	1	7	4
3364.2	220	subangular	88	1	11	0	13	3	8	28
3365.9	300	angular-subangular	85	2	13	36	3	2	8	1
3367.8	330	subangular	92	2	6	46	4	1	6	1
3368.6	230	subangular-subrounded	91	1	8	0	17	4	7	18
3369.4	180	angular-subangular	84	2	14	33	4	2	10	2
3369.9	220	angular-subangular	85	1	14	26	5	1	15	3
3371.1	240	subangular-subrounded	86	4	10	46	9	0	13	2
3372.5	240	angular-subangular	87	1	12	34	3	1	7	1
3374	350	angular-subangular	85	1	14	32	2	0	7	1
3375	220	angular-subangular	77	7	16	28	5	2	12	1
3375	230	angular-subangular	79	5	16	34	6	1	15	1
3375.85	320	subangular	79	1	20	34	5	1	16	10
3377.1	270	subangular	94	1	5	0	10	5	9	20
3377.9	310	subangular-subrounded	88	1	11	37	1	3	8	7
3379.7	300	subangular-subrounded	82	1	17	42	2	2	9	3
3381.1	320	subangular	81	1	18	40	2	6	11	2
3382.2	230	subangular-subrounded	79	1	20	3	2	2	6	17
3382.8	280	subangular	89	3	8	41	2	3	10	2
3383.4	320	subangular	83	1	16	39	2	2	8	7
3384.5	160	angular-subangular	72	10	18	19	13	0	13	12
3384.8	170	subangular	69	7	24	39	2	2	10	3
3385.7	230	subangular	74	10	16	40	3	1	9	2
3386.5	220	angular-subangular	69	8	23	41	1	1	11	1
3387.4	210	subangular	87	3	10	0	2	5	10	20
3387.8	210	subangular-subrounded	81	4	15	0	5	7	7	23
3388.9	very-fined grain									
3389.6	very-fined grain									

Note: Quartz\* + Feldspar\* + Lithic Fragment\* = 100%.

**Appendix II**

Fluid inclusion analysis of calcite cement in Ti-3 sandstones.

Sample#	Host mineral	Occurrence	Th <sup>°</sup> C	Ti <sup>°</sup> CTi <sup>°</sup> CTi <sup>°</sup> CTi <sup>°</sup> CTi <sup>°</sup> C	Tm <sup>°</sup> CTm <sup>°</sup> CTm <sup>°</sup> CTm <sup>°</sup> CTm <sup>°</sup> C	Eq.wt% NaCl (Bodnar, 2003)
Monophase1	Poikilotopic Calcite	Cluster			-0.3	0.53
Monophase2	Poikilotopic Calcite	Cluster		-40.3	-0.3	0.53
Monophase3	Poikilotopic Calcite	Cluster		-42.2	-0.4	0.70
Monophase4	Poikilotopic Calcite	Cluster			-0.5	0.88
Monophase5	Poikilotopic Calcite	Cluster			-0.6	1.05
Monophase6	Poikilotopic Calcite	Cluster			-0.7	1.22
Monophase7	Poikilotopic Calcite	Cluster		-47.9	-0.7	1.22
Monophase8	Poikilotopic Calcite	Cluster			-0.9	1.57
Monophase9	Poikilotopic Calcite	Cluster			-0.9	1.57
Monophase10	Poikilotopic Calcite	Cluster		-45.8	-1	1.74
Monophase11	Poikilotopic Calcite	Cluster			-1.3	2.24
Monophase12	Poikilotopic Calcite	Cluster		-48.3	-1.5	2.57
Monophase13	Poikilotopic Calcite	Cluster			-1.5	2.57
Monophase14	Poikilotopic Calcite	Cluster			-1.6	2.74
Monophase15	Poikilotopic Calcite	Cluster			-1.7	2.90
Monophase16	Poikilotopic Calcite	Cluster		-50.6	-1.9	3.23
Monophase17	Poikilotopic Calcite	Cluster			-2	3.39
Monophase18	Poikilotopic Calcite	Cluster		-33.8	-2	3.39
Monophase19	Poikilotopic Calcite	Cluster		-38.7	-2.1	3.55
Monophase20	Poikilotopic Calcite	Cluster			-2.6	4.34
Monophase21	Poikilotopic Calcite	Cluster			-2.7	4.49
Monophase22	Poikilotopic Calcite	Cluster			-2.7	4.49
Monophase23	Poikilotopic Calcite	Cluster		-47.4	-2.8	4.65
Monophase24	Poikilotopic Calcite	Cluster			-3	4.96
Monophase25	Poikilotopic Calcite	Cluster			-3	4.96
Monophase26	Poikilotopic Calcite	Cluster			-3.2	5.26
Monophase27	Poikilotopic Calcite	Cluster			-4	6.45
Monophase28	Poikilotopic Calcite	Cluster			-4	6.45
33446-T1	Poikilotopic Calcite	Individual	64.8	-34.7	-4.5	7.17
33446-T2	Poikilotopic Calcite	Individual	68.2		-4.6	7.31
33446-T3	Poikilotopic Calcite	Individual	65.2	-55.2	-5.1	8.00
33446-T4	Poikilotopic Calcite	Individual	63.9			
33572-T1	Poikilotopic Calcite	Individual	76.4			
33572-T2	Poikilotopic Calcite	Individual	75.9			
33572-T3	Poikilotopic Calcite	Individual	75.3			
33572-T4	Poikilotopic Calcite	Individual	76.2			
33678-T1	Poikilotopic Calcite	Individual	75.3			
33678-T2	Poikilotopic Calcite	Individual	66.3		-5.4	8.41
33678-T3	Poikilotopic Calcite	Individual	73.8			
33678-T4	Poikilotopic Calcite	Individual	68.7		-5.8	8.95
33678-T5	Poikilotopic Calcite	Individual	74.7	-46.3	-5.2	8.14
33678-T6	Poikilotopic Calcite	Individual	65.7		-5.3	8.28
3374-T1	Poikilotopic Calcite	Individual	83.1			
3374-T2	Poikilotopic Calcite	Individual	71.1	-45.2	-5.5	8.55
3374-T3	Poikilotopic Calcite	Individual	80.4			
3374-T4	Poikilotopic Calcite	Individual	64.1			
3374-T5	Poikilotopic Calcite	Individual	76.7	-53.7	-5.9	9.08
3374-T6	Poikilotopic Calcite	Individual	72.9		-6	9.21
33779-T1	Poikilotopic Calcite	Individual	66.4	-38.6	-6.9	10.36
33779-T2	Poikilotopic Calcite	Individual	77.2			
33779-T3	Poikilotopic Calcite	Individual	80.8	-53.2	-7.2	10.73
33779-T4	Poikilotopic Calcite	Individual	72			
33779-T5	Poikilotopic Calcite	Individual	67.8			
33779-T6	Poikilotopic Calcite	Individual	73.3		-7.6	11.22
33779-T7	Poikilotopic Calcite	Individual	76.6			
Fracture-T1	Fracture-filling Calcite	Individual	92	-48.3	-5.8	8.95
Fracture-T2	Fracture-filling Calcite	Individual	135	-53.9	-5.3	8.28
Fracture-T3	Fracture-filling Calcite	Individual	117.6			
Fracture-T4	Fracture-filling Calcite	Individual	138.1			
Fracture-T5	Fracture-filling Calcite	Individual	89.4		-5.3	8.28
Fracture-T6	Fracture-filling Calcite	Individual	133.2	-50.6	-9.3	13.18
Fracture-T7	Fracture-filling Calcite	Individual	76.4			
Fracture-T8	Fracture-filling Calcite	Individual	75.3			
Fracture-T9	Fracture-filling Calcite	Individual	91.6	-46.5	-5.5	8.55
Fracture-T10	Fracture-filling Calcite	Individual	105.6			
Fracture-T11	Fracture-filling Calcite	Individual	84.7			
Fracture-T12	Fracture-filling Calcite	Individual	122.3		-6	9.21
Fracture-T13	Fracture-filling Calcite	Individual	76.2			
Fracture-T14	Fracture-filling Calcite	Individual	75.9			
Fracture-T15	Fracture-filling Calcite	Individual	97.3	-52.4	-7.8	11.46
Fracture-T16	Fracture-filling Calcite	Individual	105.1		-8.3	12.05

**Appendix III**

Quantitative fluid-inclusion gas analysis of individual crushes for calcite cement of Ti-3 sandstones.

Sample	3344.8									Weighted Mean
Crush#		<b>9360a</b>	<b>9360b</b>	<b>9360c</b>	<b>9360d</b>	<b>9360e</b>	<b>9360f</b>	<b>9360g</b>	<b>9360h</b>	
H2	0.013	0.014	0.017		0.014	0.027	0.029	0.027	0.021	
He	0.000	0.000	0.000		0.000	0.001	0.000	0.001	0.000	
CH4	2.229	3.120	2.693		1.861	3.283	2.806	3.108	2.718	
H2O	95.196	92.948	94.060		94.897	91.696	92.734	92.768	93.405	
N2	0.453	0.746	0.696		0.568	1.086	0.765	0.817	0.744	
O2	0.000	0.000	0.000		0.001	0.000	0.000	0.001	0.000	
Ar	0.006	0.009	0.000		0.008	0.011	0.010	0.010	0.008	
CO2	1.128	1.965	1.267		1.251	2.112	1.853	1.448	1.564	
Sample	3344.5									Weighted Mean
Crush#		<b>9361a</b>	<b>9361b</b>	<b>9361c</b>	<b>9361d</b>	<b>9361e</b>	<b>9361f</b>	<b>9361g</b>	<b>9361h</b>	
H2	0.002	0.007	0.011	0.024	0.038	0.038	0.052	0.084	0.032	
He	0.000	0.000	0.000	0.000	0.001	0.000	0.000	0.001	0.000	
CH4	0.947	2.083	0.952	2.123	2.810	1.402	1.402	1.883	1.751	
H2O	95.357	92.479	94.418	91.564	89.596	93.691	93.113	92.264	92.599	
N2	0.448	0.778	0.632	0.868	0.941	0.668	0.617	0.827	0.739	
O2	0.004	0.000	0.059	0.001	0.000	0.003	0.006	0.002	0.009	
Ar	0.006	0.011	0.009	0.010	0.015	0.009	0.010	0.010	0.010	
CO2	2.687	3.756	3.033	4.200	5.219	3.241	3.671	3.841	3.804	
Sample	3367.8									Weighted Mean
Crush#		<b>9362a</b>	<b>9362b</b>	<b>9362c</b>	<b>9362d</b>	<b>9362e</b>	<b>9362f</b>	<b>9362g</b>	<b>9362h</b>	
H2	0.039	0.122	0.061	0.019	0.047	0.087	0.082	0.120	0.074	
He	0.000	0.001	0.000	0.000	0.001	0.000	0.001	0.001	0.001	
CH4	3.550	5.491	1.916	6.455	3.763	4.879	4.358	6.269	4.858	
H2O	87.028	83.827	90.540	87.929	89.719	87.462	86.652	83.599	87.079	
N2	2.048	2.122	0.670	0.626	0.693	0.934	1.618	1.534	1.158	
O2	0.067	0.066	0.013	0.000	0.000	0.021	0.021	0.016	0.018	
Ar	0.023	0.032	0.017	0.013	0.017	0.019	0.027	0.030	0.022	
CO2	6.201	6.194	5.552	3.772	4.094	5.199	5.264	5.766	5.036	
Sample	3377.9									Weighted Mean
Crush#		<b>9363a</b>	<b>9363b</b>	<b>9363c</b>	<b>9363d</b>	<b>9363e</b>	<b>9363f</b>	<b>9363g</b>	<b>9363h</b>	
H2	0.031	0.045	0.039	0.042	0.111	0.075	0.086	0.083	0.065	
He	0.000	0.000	0.000	0.000	0.000	0.000	0.001	0.001	0.000	
CH4	1.442	2.006	1.476	1.532	2.282	2.848	6.478	3.466	2.825	
H2O	94.916	92.402	94.941	92.767	90.842	90.778	87.091	90.776	91.807	
N2	0.507	0.641	0.324	0.809	0.884	0.630	1.082	0.798	0.702	
O2	0.010	0.007	0.006	0.011	0.037	0.000	0.009	0.007	0.009	
Ar	0.007	0.007	0.006	0.011	0.015	0.014	0.014	0.014	0.011	
CO2	2.385	4.330	2.501	4.276	5.142	3.982	4.179	3.235	3.518	
Sample	33,797									Weighted Mean
Crush#		<b>9364a</b>	<b>9364b</b>	<b>9364c</b>	<b>9364d</b>	<b>9364e</b>	<b>9364f</b>	<b>9364g</b>	<b>9364h</b>	
H2	0.188	0.066	0.090	0.059	0.030	0.119			0.091	
He	0.000	0.000	0.000	0.001	0.000	0.001			0.000	
CH4	6.906	5.869	4.900	9.290	6.668	3.296			6.429	
H2O	85.380	80.936	77.888	81.032	84.666	85.547			83.285	
N2	1.174	1.411	1.629	1.162	0.491	0.918			1.025	
O2	0.024	0.005	0.011	0.060	0.013	0.042			0.025	
Ar	0.014	0.034	0.041	0.019	0.009	0.025			0.020	
CO2	5.422	8.572	12.242	7.645	7.635	8.732			7.804	
Sample	3381.1									Weighted Mean
Crush#		<b>9365a</b>	<b>9365b</b>	<b>9365c</b>	<b>9365d</b>	<b>9365e</b>	<b>9365f</b>	<b>9365g</b>	<b>9365h</b>	
H2	0.000	0.000	0.000	0.000	0.003	0.000	0.000	0.002	0.000	
He	0.000	0.000	0.000	0.000	0.000	0.000	0.000	0.000	0.000	
CH4	0.282	0.164	0.199	0.202	0.138	0.203	0.497	0.685	0.282	
H2O	98.348	99.105	98.400	98.345	99.289	99.267	98.206	98.237	98.533	
N2	0.143	0.087	0.131	0.114	0.087	0.069	0.252	0.162	0.129	
O2	0.067	0.031	0.057	0.055	0.007	0.007	0.017	0.012	0.042	
Ar	0.003	0.001	0.002	0.002	0.001	0.001	0.003	0.001	0.002	
CO2	0.681	0.450	0.827	0.807	0.290	0.378	0.915	0.800	0.696	

**Appendix IV**

. Trace element analysis of calcite cement by SIMS.

SIMS SPOT	Fe(ppm)	Mn(ppm)	Sr(ppm)
Sample 3344.6			
A-1	120.05	595.51	498.55
A-2	68.37	568.45	1113.69
B-1	322.80	617.36	453.96
B-2	77.54	818.72	444.34
B-3	397.06	652.60	754.05
C-1	36.55		
C-2	149.62		
C-3	41.08		
D-1	176.68		
D-2	38.62		
D-3	42.66		
Sample 3367.8			
A-1	32.53	359.83	1620.84
A-2	47.40	294.91	1746.82
A-3	46.71	321.69	1771.36
A-4	51.58	373.47	1759.08
B-1	41.55		
B-2	37.83		
B-3	27.66		
B-4	29.98		
B-5	35.85		
C-1	33.27		
C-2	57.62		
Sample 3371.1			
A-1	224.90	180.60	2260.06
A-2	157.20	243.00	786.10
B-1	90.36		
B-2	201.60		
B-3	103.96		
B-4	64.86		
C-1	138.25	235.37	640.06
C-2	78.56	194.73	1395.75
D-1	62.39		
D-2	43.82		
E-1	208.40	255.53	645.17
F-1	82.57		
F-2	99.21		
Sample 3379.1			
A-1	314.70	55.15	1851.23
A-2	278.25	54.18	1910.37
A-3	250.07	55.14	1963.54
B-1	493.59		
B-2	166.27		
C-1	125.08	77.34	446.08
C-2	134.85	64.58	1324.84
C-3	151.69	58.59	1933.97
D-1	387.68		
D-2	145.28		
D-3	70.01		
D-4	254.66		
D-5	104.00		
D-6	186.21		
D-7	451.95		
D-8	83.36		
Sample 3386.5			
A-1	64.74	1629.66	1863.67
A-2	88.50	1768.73	987.55
A-3	126.49	1021.77	2217.55
A-4	46.38	1689.09	675.95
B-1	45.79		
B-2	37.76		
B-3	41.56		
B-4	33.62		
B-5	73.78		
B-6	44.12		
Standard			
oka c 1 Dec 5 2013	337.5	2340.2	13920.3
oka c 2 Dec 5 2013	343.6	2317.2	14219.1
oka_c@1	306.6	2307.0	14337.8
oka_c@2	317.5	2289.4	13751.9
oka_c@3	352.0	2308.8	13922.6
oka c1 Dec 6 2013	341.1	2086.6	14298.0
oka c2 Dec 6 2013	338.6	2544.9	13591.0

**Appendix IV (continued)**

SIMS SPOT	Fe(ppm)	Mn(ppm)	Sr(ppm)
oka_c_1_Aug_26_2014@1	394.5	2348.1	14857.5
oka_c_1_Aug_26_2014@2	361.2	2319.6	13718.9
oka_c_1_Aug_26_2014@3	324.1	2304.4	14171.9

**Appendix V**

REE concentrations of calcite cement of Ti-3 sandstones.

SIMS SPOT	La (ppm)	Ce (ppm)	Pr (ppm)	Nd (ppm)	Sm (ppm)	Eu (ppm)	Gd	Tb	Dy (ppm)	Ho	Er (ppm)	Tm	Yb (ppm)	Lu	$\Sigma$ Total REE (ppm)
<b>Sample 3344.6</b>															
A-1	5.04	7.80		3.64	0.82	0.29			0.35	0.05	0.11				18.09
A-2	2.83	5.85		3.22	0.82	0.32			0.53	0.03	0.19				13.80
A-3	1.87	3.38		2.05	0.55	0.18			0.26	0.10	0.06				8.45
B-1	2.09	4.54		2.96	0.58	0.29			0.58	0.20	0.10				11.33
B-2	2.81	6.46		3.87	1.23	0.35			0.63	0.18	0.13				15.67
B-3	5.82	10.30		4.95	1.21	0.43			0.62	0.29	0.11				23.72
<b>Sample 3367.8</b>															
A-1	0.37	1.02		0.84	0.28	0.06			0.14	na	0.04				2.76
A-2	0.46	1.29		1.16	0.35	0.08			0.10	0.03	0.02				3.49
A-3	0.25	1.02		0.75	0.35	0.05			0.14	na	0.02				2.58
A-4	0.88	1.94		1.18	0.38	0.08			0.12	0.05	0.04				4.68
B-1	0.35	1.29		0.94	0.18	0.04			0.08	0.01	na				2.88
B-2	0.79	1.50		1.08	0.35	0.10			0.09	0.03	0.04				3.98
B-3	0.54	1.45		1.01	0.31	0.07			0.13	0.01	0.01				3.52
Note: "na" means concentration that cannot be detected															
<b>Sample 3371.1</b>															
A-1	1.66	1.22		0.80	0.23	0.06			0.17	0.11	0.09				4.34
A-3	1.02	0.69		0.55	0.25	0.12			0.19	0.04	0.04				2.89
B-1	1.88	3.86		2.26	0.84	0.26			0.42	0.15	0.12				9.78
B-2	2.91	5.93		3.52	0.75	0.23			0.32	0.16	0.17				13.99
C-1	0.35	0.67		0.72	0.31	0.05			0.12	0.05	0.05				2.32
C-2	1.58	2.43		1.65	0.32	0.11			0.15	0.07	0.04				6.34
D-1	8.94	18.97		10.00	2.88	0.80			1.50	0.59	0.69				44.36
D-2	6.21	13.74		7.50	2.59	0.67			1.64	0.60	0.61				33.58
D-3	8.30	16.60		7.70	2.27	0.67			1.39	0.48	0.47				37.89
E-1	1.15	2.75		2.43	0.69	0.21			0.40	0.12	0.09				7.85
E-2	1.11	2.72		2.54	0.57	0.15			0.22	0.15	0.07				7.53
E-3	2.00	2.94		1.70	0.42	0.14			0.23	0.07	0.10				7.60
E-4	0.35	0.85		0.67	0.39	0.08			0.10	0.04	0.05				2.52
<b>Sample 3379.1</b>															
A-1	0.77	1.76		1.13	0.39	0.12			0.20	0.04	0.10				4.52
A-2	1.14	2.47		1.66	0.53	0.20			0.28	0.07	0.11				6.46
C-1	3.03	4.69		2.78	0.77	0.17			0.34	0.15	0.07				12.00
C-2	0.43	0.89		0.82	0.23	0.08			0.12	0.02	0.03				2.62
D-1	1.01	2.22		2.11	0.88	0.21			0.47	0.04	0.14				7.08
D-2	1.54	3.43		2.60	0.83	0.49			0.33	0.01	0.15				9.39
E-1	0.71	1.30		1.09	0.25	0.08			0.13	0.54	0.04				4.14
E-2	0.99	1.88		1.31	1.30	0.12			0.20	0.06	0.07				5.94
E-3	0.67	1.41		0.89	0.42	0.08			0.15	0.21	0.02				3.85
E-4	1.30	2.25		1.36	0.43	0.13			0.17	0.04	0.06				5.73
<b>Sample 3386.5</b>															
A-1	0.15	0.21		0.08	0.02	na			na	na	na				0.46
A-2	0.12	0.22		0.13	na	na			na	na	na				0.48
B-1	0.53	1.15		1.01	0.21	0.07			0.09	0.07	na				3.13
B-2	0.81	1.26		0.65	0.14	0.03			0.02	na	na				2.91
C-1	0.24	0.30		0.23	0.16	0.04			0.06	0.06	0.04				1.12
D-1	1.04	1.71		1.02	0.26	0.07			0.12	0.02	0.04				4.26
D-2	1.79	3.92		1.96	0.55	0.19			0.41	0.13	0.12				9.06
Note: "na" means concentration that cannot be detected															
<b>Standard</b>															
oka_c_Jan_22_2014@1	448.42	532.24		148.80	21.51	8.65			5.12	1.92	2.44				
oka_c_Jan_22_2014@2	447.92	533.87		152.49	22.16	10.04			4.83	2.22	2.96				
oka_c_Jan_22_2014@3	445.36	522.91		145.66	20.20	9.88			5.23	2.24	2.70				
oka_c_Jan_22_2014@5	434.65	513.65		143.76	20.85	9.37			4.79	2.06	2.77				
oka_c_Jan_22_2014@6	438.72	517.73		146.75	20.21	9.33			4.59	2.26	2.61				
oka_c_Jan_23_2014@3	436.95	518.88		140.06	20.64	7.94			5.09	2.13	2.66				
oka_c_Jan_23_2014@2	438.89	530.30		139.43	20.94	9.27			5.06	2.15	2.92				
oka_c_Jan_27_2014@3	451.77	534.83		150.67	19.93	8.76			4.90	2.13	2.62				
oka_c_Jan_27_2014@2	447.74	534.56		147.26	20.90	8.92			5.43	2.38	2.76				
oka_c_aug_27_2014@2	440.12	521.83		146.31	22.42	8.48			4.93	2.02	2.46				
oka_c_aug_27_2014@1	445.08	532.29		150.59	22.38	8.60			5.16	2.03	2.25				
Oka c 2 Aug 28 2014	460.83	542.33		142.18	22.15	7.52			5.13	2.17	2.47				
Oka c 1 Aug 28 2014	425.57	503.55		134.90	19.75	10.78			4.92	2.35	2.48				

(continued on next page)

**Appendix V (continued)**

SIMS SPOT	La (ppm)	Ce (ppm)	Pr	Nd (ppm)	Sm (ppm)	Eu (ppm)	Gd	Tb	Dy (ppm)	Ho	Er (ppm)	Tm	Yb (ppm)	Lu	$\sum$ Total REE (ppm)
oka_c_Sept_4_2014@3	441.75	522.08		149.24	21.26	8.54			4.75		2.11		2.28		
oka_c_Sept_4_2014@4	442.93	528.27		153.79	21.65	8.68			5.41		2.22		2.55		
oka_c_Sept_4_2014@5	444.02	524.66		149.39	21.77	9.01			5.32		2.28		2.79		
x	442.90	525.00		144.34	21.34	8.90			4.94		2.44		2.51		

**References**

- Alibo, D.S., Nozaki, Y., 1999. Rare earth elements in seawater: particle association, shale-normalization, and Ce oxidation. *Geochimica Cosmochimica Acta* 63, 363–372.
- Azmy, K., Blamey, N.J.F., 2013. Source of diagenetic fluids from fluid-inclusion gas ratios. *Chem. Geol.* 347, 246–254.
- Azmy, K., Brand, U., Sylvester, P., Gleeson, S.A., Logan, A., Bitner, M.A., 2011. Biogenic and abiogenic low-Mg calcite (bLMC and aLMC): evaluation of seawater-REE composition, water masses and carbonate diagenesis. *Chem. Geol.* 280, 180–190.
- Azmy, K., Knight, I., Lavoie, D., Chi, G., 2009. Origin of dolomites in the Boat Harbour Formation, St. George Group, in western Newfoundland, Canada: implications for porosity development. *Bull. Can. Petroleum Geol.* 57, 81–104.
- Azomani, E., Azmy, K., Blamey, N., Brand, U., Al-Aasm, I., 2013. Origin of Lower Ordovician dolomites in eastern Laurentia: controls on porosity and implications from geochemistry. *Mar. Petroleum Geol.* 40, 99–114.
- Baccar, M.B., Fritz, B., Made, B., 1993. Diagenetic albitionization of K-feldspar and plagioclase in sandstone reservoirs; thermodynamic and kinetic modeling. *J. Sediment. Res.* 63, 1100–1109.
- Baker, J.C., Havord, P.J., Martin, K.R., Ghori, K.A.R., 2000. Diagenesis and petrophysics of the early Permian Moogooloo sandstone, southern Carnarvon basin, western Australia. *AAPG Bull.* 84, 250–265.
- Banner, J.L., 1995. Application of the trace element and isotope geochemistry of strontium to studies of carbonate diagenesis. *Sedimentology* 42, 805–824.
- Barnaby, R.J., Rimstidt, J.D., 1989. Redox conditions of calcite cementation interpreted from Mn and Fe contents of authigenic calcites. *Geol. Soc. Am. Bull.* 101, 795–804.
- Bau, M., Balan, S., Schmidt, K., Koschinsky, A., 2010. Rare earth elements in mussel shells of the Mytilidae family as tracers for hidden and fossil high-temperature hydrothermal systems. *Earth Planet. Sci. Lett.* 299, 310–316.
- Bau, M., Dulski, P., 1996. Distribution of yttrium and rare-earth elements in the Penge and Kuruman iron-formations, Transvaal Supergroup, South Africa. *Precambrian Res.* 79, 37–55.
- Bennett, P.C., Siegel, D.I., 1987. Increased solubility of quartz in water due to complexing by organic compounds. *Nat. (Lond.)* 326, 684–686.
- Bjørkum, P.A., Walderhaug, O., 1990. Geometrical arrangement of calcite cementation within shallow marine sandstones. *Earth Sci. Rev.* 29, 145–161.
- Bjørlykke, K., Jahren, J., 2010. Sandstones and sandstone reservoirs. In: Bjørlykke, K. (Ed.), *Petroleum Geoscience: from Sedimentary Environments to Rock Physics*. Springer, Amsterdam, pp. 113–140.
- Bjørlykke, K., Ramm, M., Saigal, G.C., 1989. Sandstone diagenesis and porosity modification during basin evolution. *Geol. Rundsch.* 78, 243–268.
- Blamey, N.J.F., 2012. Composition and evolution of crustal, geothermal and hydrothermal fluids interpreted using quantitative fluid inclusion gas analysis. *J. Geochem. Explor.* 116, 17–27.
- Blamey, N.J.F., Azmy, K., Brand, U., 2014. Provenance and burial history of cement in sandstones of the Northbrook Formation (Carboniferous), western Newfoundland, Canada: a geochemical investigation. *Sediment. Geol.* 299, 30–41.
- Blamey, N., Norman, D.I., 2002. New interpretations of geothermal fluid inclusion volatiles: Ar/He and N2/Ar ratios—A better indicator of magmatic volatiles, and equilibrium gas geothermometry. In: *Proceedings: Twenty-seventh Workshop on Geothermal Reservoir Engineering*. Stanford University, Stanford, California.
- Bodnar, R.J., 2003. Interpretation of data from aqueous-electrolyte fluid inclusion. In: Samson, I., Anderson, A., Marshal, D. (Eds.), *Fluid Inclusions: Analysis and Interpretation*. Mineralogical Association of Canada Short Course 32, pp. 81–100.
- Boggs, S., Krinsley, D., 2006. Application of Cathodoluminescence Imaging to the Study of Sedimentary Rocks. Cambridge University Press, New York.
- Brehm, U., Gorbushina, A., Mottershead, D., 2005. The role of microorganisms and biofilms in the breakdown and dissolution of quartz and glass. *Palaeogeogr. Palaeoclimatol. Palaeoecol.* 219, 117–129.
- Brown, D.M., McAlpine, K.D., Yole, R.W., 1989. Sedimentology and sandstone diagenesis of Hibernia Formation in Hibernia oil field, Grand Banks of Newfoundland. *AAPG Bull.* 73, 557–575.
- Burley, S.D., Kantorowicz, J.D., 1986. Thin section and SEM textural criteria for the recognition of cement-dissolution porosity in sandstones. *Sedimentology* 33, 587–604.
- Clark, I.D., Fritz, P., 1997. Environmental Isotopes in Hydrogeology. Lewis, New York.
- Conilffe, J., Azmy, K., Gleeson, S.A., Lavoie, D., 2010. Fluids associated with hydrothermal dolomitization in St. George Group, western Newfoundland, Canada. *Geofluids* 10, 422–437.
- de Baar, H.J.W., Bacon, M.P., Brewer, P.G., Bruland, K.W., 1985. Rare earth elements in the Pacific and Atlantic Oceans. *Geochimica Cosmochimica Acta* 49, 1943–1959.
- de Baar, H.J.W., German, C.R., Elderfield, H., Van Gaans, P., 1988. Rare earth element distributions in anoxic waters of the Cariaco Trench. *Geochimica et Cosmochimica Acta* 52, 1203–1219.
- Denniston, R.F., Shearer, C.K., Layne, G.D., Vaniman, D.T., 1997. SIMS analyses of minor and trace element distributions in fracture calcite from Yucca Mountain, Nevada, USA. *Geochimica Cosmochimica acta* 61, 1803–1818.
- Desilva, N.R., 2000. Flemish Pass Basin: hydrocarbon prospectivity and potential deep water development. *Terra Nova* 64, 2–2.
- DeSilva, N.R., 1999. Sedimentary basins and petroleum systems offshore Newfoundland and Labrador. In: Fleet, A.J., Boldy, S.A.R. (Eds.), *Petroleum Geology of Northwest Europe: Proceedings of the Fifth Conference*. The Geological Society, London, pp. 501–515.
- Dickson, T., 1990. Carbonate mineralogy and chemistry. In: Tucker, M.E., Wright, V.P. (Eds.), *Carbonate Sedimentology*. Blackwell Scientific Publications, Oxford, pp. 284–313.
- Dutton, S.P., 2008. Calcite cement in Permian deep-water sandstones, Delaware Basin, west Texas: origin, distribution, and effect on reservoir properties. *AAPG Bull.* 92, 765–787.
- Dutton, S.P., Loucks, R.G., Day-Stirrat, R.J., 2012. Impact of regional variation in detrital mineral composition on reservoir quality in deep to ultradeep lower Miocene sandstones, western Gulf of Mexico. *Mar. Petroleum Geol.* 35, 139–153.
- Dutton, S.P., Willis, B.J., White, C.D., Bhattacharya, J.P., 2000. Outcrop characterization of reservoir quality and interwell-scale cement distribution in a tide-influenced delta, Frontier Formation, Wyoming, USA. *Clay Miner.* 35, 95–105.
- Elderfield, H., Greaves, M.J., 1982. The rare earth elements in seawater. *Nature* 296, 214–218.
- Enachescu, M.E., 1987. Tectonic and structural framework of the northeast Newfoundland continental margin. In: Beaumont, C., Tankard, A.J. (Eds.), *Sedimentary Basins and Basin Forming Mechanisms*. Canadian Society of Petroleum Geologists, Memoirs 12, pp. 117–146.
- Enachescu, M.E., 1988. Extended basement beneath the intracratonic rifted basins of the Grand Banks of Newfoundland. *Can. J. Explor. Geophys.* 24, 48–65.
- Enachescu, M., 2012. Petroleum Exploration Opportunities in the Flemish Pass Basin. Call for Bids NL12-02, Parcel 1. [http://www.nr.gov.nl.ca/nr/invest/call\\_bids\\_petro\\_exploration\\_enachescu%20.pdf](http://www.nr.gov.nl.ca/nr/invest/call_bids_petro_exploration_enachescu%20.pdf).
- Enachescu, M., 2014. Petroleum Exploration Opportunities in the Flemish Pass Basin. Newfoundland and Labrador Offshore Area: Call for Bids NL13-01, Area "C"—Flemish Basin, Parcel. <http://www.nr.gov.nl.ca/nr/invest/nl1301flemishpassbasinenachescu.pdf>.
- Enachescu, M.E., Hogg, J.R., Fowler, M., Brown, D.E., Atkinson, I., 2010. Late Jurassic Source Rock Super-highway on Conjugate Margins of the North and Central Atlantic (Offshore East Coast Canada, Ireland, Portugal, Spain and Morocco). CM 2010-Abstracts, 2.
- Enachescu, M.E., Kearsey, S., Hardy, V., Sibuet, J., Hogg, J., Srivastava, S., Fagan, A., Thompson, T., Ferguson, R., 2005. Evolution and petroleum potential of Orphan Basin, offshore Newfoundland, and its relation to the movement and rotation of Flemish Cap based on plate kinematics of the North Atlantic. In: Post, P.J.R., Norman, C., Olson, S.L., Plumes, S.L., Lyons, K.T., Newton, G.B. (Eds.), 25th Annual Gulf Coast Section SEPM Foundation, Bob F. Perkins Research Conference, Symposium on Petroleum Systems of Divergent Continental Margin Basins, Society for Sedimentary Geology, Gulf Coast Section 25, Dallas, Texas, pp. 7–8.
- Epstein, S.A., Friedman, G.M., 1982. Processes controlling precipitation of carbonate cement and dissolution of silica in reef and near-reef settings. *Sediment. Geol.* 33, 157–171.
- Faure, G., Mensing, T.M., 2005. *Isotopes: Principles and Applications*. John Wiley & Sons Inc., Hoboken, New Jersey.
- Folk, R.L., 1980. *Petrology of Sedimentary Rocks*. Hemphill Publishing Co., Austin, Texas.
- Foster, D.G., Robinson, A.G., 1993. Geological history of the Flemish Pass Basin, offshore Newfoundland. *AAPG Bull.* 77, 588–609.
- Frank, J.R., Carpenter, A.B., Oglesby, T.W., 1982. Cathodoluminescence and composition of calcite cement in the Taum Sauk Limestone (Upper Cambrian), Southeast Missouri. *J. Sediment. Res.* 52, 631–638.
- Friedman, G.M., Ali, S.A., Krinsley, D.H., 1976. Dissolution of quartz accompanying carbonate precipitation and cementation in reefs; example from the Red Sea. *J. Sediment. Res.* 46, 970–973.
- Friedman, I., O'Neil, J.R., 1977. Compilation of stable isotope fractionation factors of geochemical interest. In: Fleischer, M. (Ed.), *Data of Geochemistry*. USGPO, Washington, D.C, pp. 1–12.

- García-García, F., Marfil, R., De Gea, G.A., Delgado, A., Kobstädt, A., Santos, A., Mayoral, E., 2013. Reworked marine sandstone concretions: a record of high-frequency shallow burial to exhumation cycles. *Facies* 59, 843–861.
- German, C.R., Elderfield, H., 1990. Application of the Ce anomaly as a paleoredox indicator: the ground rules. *Paleoceanography* 5, 823–833.
- Giggenbach, W.F., 1986. The use of gas chemistry in delineating the origin of fluids discharges over the Taupo Volcanic Zone. In: International Volcanological Congress, Hamilton, New Zealand, pp. 47–50.
- Gladney, E.S., O'Malley, B.T., Roelandts, I., Gills, T.E., 1987. Compilation of Elemental Concentration Data for NBS Clinical, Biological, Geological, and Environmental Standard Reference Materials. NBS Special Report 260–111.
- Goldstein, S.J., Jacobsen, S.B., 1988. Rare earth elements in river waters. *Earth Planet Sci. Lett.* 89, 35–47.
- Goldstein, R.H., Reynolds, T.J., 1994. Systematics of Fluid Inclusions in Diagenetic Minerals. Society for Sedimentary Geology Short Course Notes 31, p. 199.
- González-Acebrón, L., Arribas, J., Mas, R., 2010. Role of sandstone provenance in the diagenetic albitionization of feldspars: a case study of the Jurassic Tera Group sandstones (Cameros Basin, NE Spain). *Sediment. Geol.* 229, 53–63.
- Gorbushina, A.A., Palinska, K.A., 1999. Biodeteriorative processes on glass: experimental proof of the role of fungi and cyanobacteria. *Aerobiologia* 15, 183–192.
- Haynes, S.R., Gruschwitz, K., Johnson, T., McDonough, M., Stacey, E., 2012. Mizzen – an Overview of the First Oil Discovery in the Flemish Pass Basin, East Coast Offshore Newfoundland, Atlantic Continental Margin. Third Conjugate Margins Conference 2012, Central and North Atlantic, Trinity College, Dublin, Ireland, Abstract Volume, p. 51.
- Haynes, S.R., Marshall, J., Imsland-Wathne, E., Minielly, G., Mortlock, E., Walderhaug, O., Johnson, T., 2013. Depositional interpretation and reservoir characterization of the lithofan in mizzen F-09, Flemish Pass Basin, Canada. In: Abstracts of Integration: CSEG, CSPG and CWLS GeoConvention 2013, Calgary, Canada.
- Hesse, R., Abid, L.A., 1998. Carbonate cementation—the key to reservoir properties of four sandstone levels (Cretaceous) in the Hibernia Oilfield, Jeanne d'Arc Basin, Newfoundland, Canada. In: Morad, S. (Ed.), Carbonate Cementation in Sandstones: Distribution Patterns and Geochemical Evolution, International Association of Sedimentologists Special Publication 26, pp. 363–393.
- Heydari, E., Moore, C.H., 1993. Zonation and geochemical patterns of burial calcite cements; upper Smackover Formation, Clarke County, Mississippi. *J. Sediment. Res.* 63, 44–60.
- Hogg, J.R., Enachescu, M.E., 2007. Exploration potential of the deep-water petroleum systems of Newfoundland and Labrador Margins. In: Offshore Technology Conference, Houston, Texas.
- Holmden, C., Hudson, J.D., 2003.  $^{87}\text{Sr}/^{86}\text{Sr}$  and Sr/Ca investigation of Jurassic mollusks from Scotland: implications for paleosalinities and the Sr/Ca ratio of seawater. *Geol. Soc. Am. Bull.* 115, 1249–1264.
- Hongo, Y., Nozaki, Y., 2001. Rare earth element geochemistry of hydrothermal deposits and Calyptogena shell from the Iheya Ridge vent field, Okinawa Trough. *Geochem. J.* 35, 347–354.
- Huppertz, T.J., Piper, D.J., 2009. The influence of shelf-crossing glaciation on continental slope sedimentation, Flemish Pass, eastern Canadian continental margin. *Mar. Geol.* 265, 67–85.
- Hutcheon, I., Nahnybida, C., Krouse, H.R., 1985. The geochemistry of carbonate cements in the Avalon sand, Grand Banks of Newfoundland. *Mineral. Mag.* 49, 457–467.
- Irwin, H., Coleman, M., Curtis, C.D., 1977. Isotopic evidence for source of diagenetic carbonates formed during burial of organic-rich sediments. *Nature* 269, 209–213.
- Kennard, L., Schafer, C., Carter, L., 1990. Late Cenozoic evolution of Sackville Spur: a sediment drift on the Newfoundland continental slope. *Can. J. Earth Sci.* 27, 863–878.
- Kinsman, D.J., 1969. Interpretation of  $\text{Sr}^{+2}$  concentrations in carbonate minerals and rocks. *J. Sediment. Res.* 39, 486–508.
- Land, L.S., 1995. Oxygen and carbon isotopic composition of Ordovician brachiopods: implications for coeval seawater: discussion. *Geochimica Cosmochimica Acta* 59, 2843–2844.
- Lawler, J.P., Crawford, M.L., 1983. Stretching of fluid inclusions resulting from a low-temperature microthermometric technique. *Econ. Geol.* 78, 527–529.
- Lee, S.G., Lee, D.H., Kim, Y., Chae, B.G., Kim, W.Y., Woo, N.C., 2003. Rare earth elements as indicators of groundwater environment changes in a fractured rock system: evidence from fracture-filling calcite. *Appl. Geochem.* 18, 135–143.
- Lindholm, R.C., Finkelman, R.B., 1972. Calcite staining: semiquantitative determination of ferrous iron: Notes. *J. Sediment. Res.* 42.
- Liu, S., Huang, S., Shen, Z., Lü, Z., Song, R., 2014. Diagenetic fluid evolution and water-rock interaction model of carbonate cements in sandstone: an example from the reservoir sandstone of the Fourth Member of the Xujiahe Formation of the Xiaoquan-Fenggu area, Sichuan Province, China. *Sci. China Earth Sci.* 57, 1077–1092.
- Longstaffe, F.J., Calvo, R., Ayalon, A., Donaldson, S., 2003. Stable isotope evidence for multiple fluid regimes during carbonate cementation of the Upper Tertiary Hazeva Formation, Dead Sea Graben, southern Israel. *J. Geochem. Explor.* 80, 151–170.
- Loucks, R.G., Bebout, D.G., Galloway, W.E., 1977. Relationship of porosity formation and preservation to sandstone consolidation history—Gulf Coast lower Tertiary Frio Formation (1). *Gulf Coast Assoc. Geol. Soc. Trans.* 27, 109–120.
- Lowe, D.G., Sylvester, P.J., Enachescu, M.E., 2011. Provenance and paleodrainage patterns of Upper Jurassic and Lower Cretaceous synrift sandstones in the Flemish Pass Basin, offshore Newfoundland, east coast of Canada. *AAPG Bull.* 95, 1295–1320.
- Lundgard, P.D., 1992. Sandstone porosity loss; a “big picture” view of the importance of compaction. *J. Sediment. Res.* 62, 250–260.
- Machel, H.G., Mason, R.A., Mariano, A.N., Mucci, A., 1991. Causes and emission of luminescence in calcite and dolomite. In: Barker, C.E., Kopp, O.C. (Eds.), Luminescence Microscopy: Quantitative and Qualitative Aspects, Society of Economic Paleontologists and Mineralogists, Short Course notes 25, pp. 9–25.
- McBride, E.F., 1989. Quartz cement in sandstones: a review. *Earth Sci. Rev.* 26, 69–112.
- McBride, E.F., Milliken, K.L., Cavazza, W., Cibin, U., Fontana, D., Picard, M.D., Zuffa, G.G., 1995. Heterogeneous distribution of calcite cement at the outcrop scale in Tertiary sandstones, northern Apennines, Italy. *AAPG Bull.* 79, 1044–1062.
- McBride, E.F., Picard, M.D., Milliken, K.L., 2003. Calcite-cemented concretions in Cretaceous sandstone, Wyoming and Utah, USA. *J. Sediment. Res.* 73, 462–483.
- McDonough, M.R., Sylvester, P., Bruder, N., Lo, J., O'Sullivan, P., 2011. Provenance of Reservoir Sandstones in the Flemish Pass and Orphan Basins (Canada): U-Pb Dating of Detrital Zircons Using the Laser Ablation Method. CM 2010-Abstracts, 5.
- McLennan, S.M., 1989. Rare earth elements in sedimentary rocks: influence of provenance and sedimentary processes. In: Lipin, B.R., McKay, G.A. (Eds.), Geochemistry and Mineralogy of Rare Earth Elements: Reviews in Mineralogy. Mineralogical Society of America, pp. 169–200.
- Morad, S., 1998. Carbonate cementation in sandstones: distribution patterns and geochemical evolution. In: Morad, S. (Ed.), Cementation in Sandstones: Distribution Patterns and Geochemical Evolution, International Association of Sedimentologists Special Publication 26, pp. 1–26.
- Morad, S., Al-Ramadan, K., Ketzer, J.M., De Ros, L.F., 2010. The impact of diagenesis on the heterogeneity of sandstone reservoirs: a review of the role of depositional facies and sequence stratigraphy. *AAPG Bull.* 94, 1267–1309.
- Morad, S., Bergan, M., Knarud, R., Nystrøm, J.P., 1990. Albitionization of detrital plagioclase in Triassic reservoir sandstones from the Snorre Field, Norwegian North Sea. *J. Sediment. Res.* 60, 411–425.
- Mozley, P.S., Burns, S.J., 1993. Oxygen and carbon isotopic composition of marine carbonate concretions: an overview. *J. Sediment. Res.* 63, 73–83.
- Norman, D.I., Blamey, N.J.F., 2001. Quantitative analysis of fluid inclusion volatiles by a two mass spectrometer system. In: Noronha, F., Doria, A., Guedes, A. (Eds.), European Current Research on Fluid Inclusions, Porto 2001 (XVI ECROFI): Faculdade de Ciencias do Porto, Departamento de Geologia, Memoria 7, pp. 341–344.
- Norman, D.I., Moore, J.N., 1997. Gaseous Species in Fluid Inclusions: a Fluid Tracer and Indicator of Fluid Processes. European Current Research on Fluid Inclusions, No. XIV, Nancy, France, Abstracts, pp. 243–244.
- Norman, D.I., Moore, J.N., 1999. Methane and excess N2 and Ar in geothermal fluid inclusions. In: Proceedings: Twenty-fourth Workshop of Geothermal Reservoir Engineering, Stanford University, Stanford, California, pp. 233–240.
- Norman, D.I., Musgrave, J.A., 1994. N 2-Ar-He compositions in fluid inclusions: indicators of fluid source. *Geochimica Cosmochimica Acta* 58, 1119–1131.
- Norman, D.I., Blamey, N., Moore, J.N., 2002. Interpreting geothermal processes and fluid sources from fluid inclusion organic compounds and CO2/N2 ratios. In: Proceedings: Twenty-seventh Workshop on Geothermal Reservoir Engineering Stanford University, Stanford, California.
- Normore, L.S., 2006. Origin, Distribution and Paragenetic Sequence of Carbonate Cements in the Ben Nevis Formation, White Rose Field, Jeanne d'Arc Basin, Offshore Newfoundland, Canada. Unpublished Master's thesis. Memorial University of Newfoundland, St. John's, Canada, p. 214.
- Nothdurft, L.D., Webb, G.E., Kamber, B.S., 2004. Rare earth element geochemistry of Late Devonian reefal carbonates, Canning Basin, Western Australia: confirmation of a seawater REE proxy in ancient limestones. *Geochimica Cosmochimica Acta* 68, 263–283.
- Nyman, S.L., Gani, M.R., Bhattacharya, J.P., Lee, K., 2014. Origin and Distribution of Calcite Concretions in Cretaceous Wall Creek Member, Wyoming: reservoir-quality implication for shallow-marine deltaic strata. *Cretac. Res.* 48, 139–152.
- Odigi, M.I., Amajor, L.C., 2010. Geochemistry of carbonate cements in Cretaceous sandstones, southeast Benue Trough, Nigeria: implications for geochemical evolution of formation waters. *J. Afr. Earth Sci.* 57, 213–226.
- Olanipekun, B.J., Azmy, K., Brand, U., 2014. Dolomites of the Boat Harbour Formation in the Northern Peninsula, western Newfoundland, Canada: implications for dolomitization history and porosity control. *AAPG Bull.* 98, 765–791.
- Parnell, J., Middleton, D., Honghan, C., Hall, D., 2001. The use of integrated fluid inclusion studies in constraining oil charge history and reservoir compartmentation: examples from the Jeanne d'Arc Basin, offshore Newfoundland. *Mar. Petroleum Geol.* 18, 535–549.
- Percival, C.J., 1983. The Firestone Sill ganister, Namurian, Northern England—the A2 horizon of a podzol or podzolic palaeosol. *Sediment. Geol.* 36, 41–49.
- Raiswell, R., 1987. Non-steady state microbiological diagenesis and the origin of concretions and nodular limestones. In: Marshall, J.D. (Ed.), Diagenesis of Sedimentary Sequences, Geological Society Special Publication 36, pp. 41–54.
- Saigal, G.C., Bjørlykke, K., 1987. Carbonate cements in clastic reservoir rocks from offshore Norway—relationships between isotopic composition, textural development and burial depth. In: Marshall, J.D. (Ed.), Diagenesis of Sedimentary Sequences, Geological Society Special Publications 36, pp. 313–324.
- Scotchman, I.C., 1991. The geochemistry of concretions from the Kimmeridge Clay Formation of southern and eastern England. *Sedimentology* 38, 79–106.

- Seyedolali, A., Krinsley, D.H., Boggs, S., O'Hara, P.F., Dypvik, H., Goles, G.G., 1997. Provenance interpretation of quartz by scanning electron microscope–cathodoluminescence fabric analysis. *Geology* 25, 787–790.
- Shepherd, T.J., Rankin, A.H., Alderton, D.H.M., 1985. A Practical Guide to Fluid Inclusions. Blackie, London, UK.
- Sholkovitz, E.R., Landing, W.M., Lewis, B.L., 1994. Ocean particle chemistry: the fractionation of rare earth elements between suspended particles and seawater. *Geochimica Cosmochimica Acta* 58, 1567–1579.
- Sinclair, I.K., 1993. Tectonism: the dominant factor in mid-Cretaceous deposition in the Jeanne d'Arc Basin, Grand Banks. *Mar. Petroleum Geol.* 10, 530–549.
- Sinclair, I.K., 1995. Sequence stratigraphic response to Aptian-Albian rifting in conjugate margin basins: a comparison of the Jeanne d'Arc Basin, offshore Newfoundland, and the Porcupine Basin, offshore Ireland. In: Geological Society Special Publications 90, pp. 29–49.
- Statoil Canada Resources, 2011. Mizzen F-09-end of Well Report. C-NLOPB file record number INV-119385. Available at the C-NLOPB library, TD Place, 140 Water Street, St. John's, Newfoundland, Canada, p. 195.
- Sverjensky, D.A., 1984. Europium redox equilibria in aqueous solution. *Earth Planet. Sci. Lett.* 67, 70–78.
- Tankard, A.J., Welsink, H.J., 1989. Mesozoic extension and styles of basin formation in Atlantic Canada. Extensional tectonics and stratigraphy of the North Atlantic Margins. *AAPG Mem.* 46, 175–195.
- Taylor, K.G., Gawthorpe, R.L., Curtis, C.D., Marshall, J.D., Awwiller, D.N., 2000. Carbonate cementation in a sequence-stratigraphic framework: upper Cretaceous sandstones, Book Cliffs, Utah–Colorado. *J. Sediment. Res.* 70, 360–372.
- Taylor, T.R., 1990. The influence of calcite dissolution on reservoir porosity in Miocene sandstones, Picaroon Field, offshore Texas Gulf Coast. *J. Sediment. Res.* 60, 322–334.
- Thomas, C., Graham, C., Ellam, R., Fallick, A., 2004.  $^{87}\text{Sr}/^{86}\text{Sr}$  chemostratigraphy of Neoproterozoic Dalradian limestones of Scotland and Ireland: constraints on depositional ages and time scales. *J. Geol. Soc.* 161, 229–242.
- Van Keer, I., Muchez, P., Viaene, W., 1998. Clay mineralogical variations and evolutions in sandstone sequences near a coal seam and shales in the Westphalian of the Campine Basin (NE Belgium). *Clay Miner.* 33, 159–169.
- Veizer, J., Ala, D., Azmy, K., Bruckschen, P., Buhl, D., Bruhn, F., et al., 1999.  $^{87}\text{Sr}/^{86}\text{Sr}$ ,  $\delta^{13}\text{C}$  and  $\delta^{18}\text{O}$  evolution of Phanerozoic seawater. *Chem. Geol.* 161, 59–88.
- Walderhaug, O., 1990. A fluid inclusion study of quartz-cemented sandstones from offshore mid-Norway; possible evidence for continued quartz cementation during oil emplacement. *J. Sediment. Res.* 60, 203–210.
- Walker, T.R., 1960. Carbonate replacement of detrital crystalline silicate minerals as a source of authigenic silica in sedimentary rocks. *Geol. Soc. Am. Bull.* 71, 145–152.
- Wanas, H.A., 2008. Calcite-cemented concretions in shallow marine and fluvial sandstones of the Birket Qarun Formation (Late Eocene), El-Faiyum depression, Egypt: field, petrographic and geochemical studies: implications for formation conditions. *Sediment. Geol.* 212, 40–48.
- Worden, R.H., Morad, S., 2000. Quartz cementation in oil field sandstones: a review of the key controversies. Quartz cementation in sandstones. *Int. Assoc. Sedimentologists Special Publ.* 29, 1–20.
- Zaid, S.M., Al Gahtani, F., 2015. Provenance, diagenesis, tectonic setting, and geochemistry of Hawkesbury Sandstone (Middle Triassic), southern Sydney Basin, Australia. *Turk. J. Earth Sci.* 24, 72–98.
- Zhong, S., Mucci, A., 1995. Partitioning of rare earth elements (REEs) between calcite and seawater solutions at 25 °C and 1 atm, and high dissolved REE concentrations. *Geochimica Cosmochimica Acta* 59, 443–453.